A Similarity Renormalization Group Approach to Green's Function Methods

Antoine Marie* and Pierre-François Loos*

Read Online

ACCESS | Metrics & More | Article Recommendations | Supporting Information

ABSTRACT: The family of Green's function methods based on the *GW* approximation has gained popularity in the electronic structure theory thanks to its accuracy in weakly correlated systems combined with its cost-effectiveness. Despite this, self-consistent versions still pose challenges in terms of convergence. A recent study [Monino and Loos *J. Chem. Phys.* **2022**, *156*, 231101.] has linked these convergence issues to the intruder-state problem. In this work, a perturbative analysis of the similarity renormalization group (SRG) approach is performed on Green's function methods. The SRG formalism enables us to derive, from first-principles, the expression of a naturally static and Hermitian form of the self-energy that can be employed in quasiparticle self-consistent *GW* (qs*GW*) calculations. The resulting SRG-based regularized self-energy significantly accelerates the convergence of qs*GW* calculations, slightly improves the overall accuracy, and is straightforward to implement in existing code.
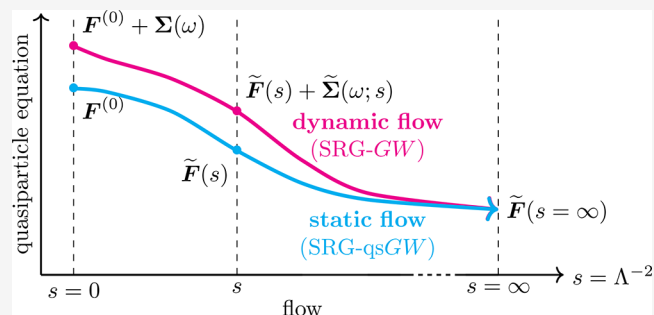
I. INTRODUCTION

The one-body Green's function provides a natural and elegant way to access the charged excitation energies of a physical system.[1−4] The nonlinear Hedin equations consist of a closed set of equations leading to the exact interacting one-body Green's function and, therefore, to a wealth of properties such as the total energy, density, ionization potentials, and electron affinities, as well as spectral functions, without the explicit knowledge of the wave functions associated with the neutral and charged electronic states of the system.[5] Unfortunately, solving exactly Hedin's equations is usually out of reach, and one must resort to approximations. In particular, the *GW* approximation,[4−9] which has been first introduced in the context of solids[10−19] and is now widely applied to molecular systems,[20−46] yields accurate charged excitation energies for weakly correlated systems[9,47−51] at a relatively low computational cost.[52−58]

The *GW* method approximates the self-energy Σ which relates the exact interacting Green's function G to a noninteracting reference version G_0 through a Dyson equation of the form

$$G(1, 2) = G_0(1, 2) + \int d(34) G_0(1, 3) \Sigma(3, 4) G(4, 2) \tag{1}$$

where $1 = (\boldsymbol{x}_1, t_1)$ is a composite coordinate gathering spin-space and time variables. The self-energy encapsulates all the Hartree-exchange-correlation effects which are not taken into account in the reference system. Approximating Σ as the first-order term of its perturbative expansion with respect to the screened Coulomb potential W yields the so-called *GW* approximation[3,5]

$$\Sigma(1, 2) = iG(1, 2) W(1, 2) \tag{2}$$

Diagrammatically, *GW* involves a resummation of the (time-dependent) direct ring diagrams via the computation of the random-phase approximation (RPA) polarizability[59,60] and is thus particularly well suited for weak correlation.

Despite a wide range of successes, many-body perturbation theory has well-documented limitations.[48,57,61−68] For example, modeling core−electron spectroscopy requires core ionization energies which have been proven to be challenging for routine *GW* calculations.[49,69−71] Many-body perturbation theory can also be used to access optical excitation energies through the Bethe-Salpeter equation.[35,41,72,73] However, the accuracy is not yet satisfying for triplet excited states, where instabilities often occur.[27,30,31,42] Therefore, even if *GW* offers a good trade-off between accuracy and computational cost, some situations might require higher precision. Unfortunately, defining a systematic way to go beyond *GW* via the inclusion of vertex corrections has been demonstrated to be a tricky task.[47,74−92] For example, Lewis and Berkelbach have shown that naive vertex corrections can even worsen the quasiparticle energies with respect to *GW*.[93] We refer the reader to the recent review by
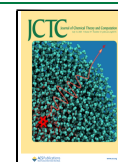
Golze and co-workers[4] for an extensive list of current challenges in Green's function methods.

Many-body perturbation theory also suffers from the infamous intruder-state problem,[94−99] where they manifest themselves as solutions of the quasiparticle equation with non-negligible spectral weights. In some cases, this transfer of spectral weight makes it difficult to distinguish between a quasiparticle and a satellite. These multiple solutions hinder the convergence of partially self-consistent schemes,[55,100,101] such as eigenvalue-only self-consistent $GW^{102−106}$ (evGW) and quasiparticle self-consistent $GW^{105,107−110}$ (qsGW). The simpler one-shot G_0W_0 scheme[10,14,18,102,111−115] is also impacted by these intruder states, leading to discontinuities and/or irregularities in a variety of physical quantities including charged and neutral excitation energies as well as correlation and total energies.[44,100,101,116−119] These convergence problems and discontinuities can even happen in the weakly correlated regime where the GW approximation is supposed to be valid.

In a recent study, Monino and Loos showed that the discontinuities could be removed by the introduction, in the quasiparticle equation, of a regularizer inspired by the similarity renormalization group (SRG).[101] Encouraged by this study and the recent successes of regularization schemes in many-body quantum chemistry methods, such as in single- and multi-reference perturbation theory,[120−125] the present work investigates the application of the SRG formalism in GW-based methods. In particular, we focus here on the possibility of curing the qsGW convergence issues using the SRG.

The SRG formalism has been developed independently by Wegner[126] in the context of condensed matter systems and Glazek and Wilson[127,128] in light-front quantum field theory. This formalism has been introduced in quantum chemistry by White[129] before being explored in more detail by Evangelista and co-workers in the context of multireference electron correlation theories.[122,123,130−137] The SRG has also been successful in the context of nuclear structure theory, where it was first developed as a mature computational tool thanks to the work of several research groups.[138−145] See ref 142 for a recent review in this field.

The SRG transformation aims at decoupling an internal (or reference) space from an external space while incorporating information about their coupling in the reference space. This process often results in the appearance of intruder states.[122,123] However, the SRG is particularly well-suited to avoid these because the decoupling of each external configuration is inversely proportional to its energy difference with the reference space. By definition, intruder states have energies that are close to the reference energy and, therefore, are the last to be decoupled. By stopping the SRG transformation once all external configurations except the intruder states have been decoupled, correlation effects between the internal and external spaces can be incorporated (or folded) without the presence of intruder states.

The goal of this manuscript is to determine if the SRG formalism can effectively address the issue of intruder states in many-body perturbation theory, as it has in other areas of electronic and nuclear structure theory. This open question will lead us to an intruder-state-free static approximation of the self-energy derived from first-principles that can be employed in partially self-consistent GW calculations. Note that throughout the manuscript we focus on the GW approximation, but the subsequent derivations can be straightforwardly applied to other self-energies such as the one derived from second-order Green's function[146−162] or the T-matrix approximation.[78,80,89,163−174]

The manuscript is organized as follows. We begin by reviewing the GW approximation in Sec. II and then briefly introduce the SRG formalism in Sec. III. A perturbative analysis of SRG applied to GW is presented in Sec. IV. The computational details are provided in Sec. V before turning to the results (Sec. VI). Our conclusions are drawn in Sec. VII. Unless otherwise stated, atomic units are used throughout.

II. THE GW APPROXIMATION

The central equation of many-body perturbation theory based on Hedin's equations is the so-called dynamical and non-Hermitian quasiparticle equation which, within the GW approximation, reads

$$[\boldsymbol{F} + \boldsymbol{\Sigma}(\omega = \epsilon_p)]\psi_p(\boldsymbol{x}) = \epsilon_p \psi_p(\boldsymbol{x}) \tag{3}$$

where $\boldsymbol{F}$ is the Fock matrix in the orbital basis,[148] and $\boldsymbol{\Sigma}(\omega)$ is (the correlation part of) the GW self-energy. Both are $K \times K$ matrices with K being the number of one-electron orbitals. Throughout the manuscript, the indices p, q, r, and s are general orbitals, while i, j, k, and l and a, b, c, and d refer to occupied and virtual orbitals, respectively. The indices μ and ν are composite indices, that is, $\nu = (ia)$, referring to neutral (single) excitations.

The self-energy can be physically understood as a correction to the Hartree−Fock (HF) problem (represented by $\boldsymbol{F}$) accounting for dynamical screening effects. Similar to the HF case, eq 3 has to be solved self-consistently, but the dynamical and non-Hermitian nature of $\boldsymbol{\Sigma}(\omega)$, as well as its functional form, makes it much more challenging to solve from a practical point of view.

The matrix elements of $\boldsymbol{\Sigma}(\omega)$ have the following closed-form expression[81,175−178]

$$\Sigma_{pq}(\omega) = \sum_{i\nu} \frac{W_{pi}^{\nu} W_{qi}^{\nu}}{\omega - \epsilon_i + \Omega_{\nu} - i\eta} + \sum_{a\nu} \frac{W_{pa}^{\nu} W_{qa}^{\nu}}{\omega - \epsilon_a - \Omega_{\nu} + i\eta} \tag{4}$$

where η is a positive infinitesimal, and the screened two-electron integrals are

$$W_{pq}^{\nu} = \sum_{ia} \langle pi|qa \rangle (\boldsymbol{X} + \boldsymbol{Y})_{ia}^{\nu} \tag{5}$$

with $\boldsymbol{X}$ and $\boldsymbol{Y}$ the components of the eigenvectors of the direct (i.e., without exchange) RPA problem defined as

$$\begin{pmatrix} \boldsymbol{A} & \boldsymbol{B} \\ -\boldsymbol{B} & -\boldsymbol{A} \end{pmatrix} \begin{pmatrix} \boldsymbol{X} & \boldsymbol{Y} \\ \boldsymbol{Y} & \boldsymbol{X} \end{pmatrix} = \begin{pmatrix} \boldsymbol{X} & \boldsymbol{Y} \\ \boldsymbol{Y} & \boldsymbol{X} \end{pmatrix} \begin{pmatrix} \boldsymbol{\Omega} & \boldsymbol{0} \\ \boldsymbol{0} & -\boldsymbol{\Omega} \end{pmatrix} \tag{6}$$

with

$$A_{ia,jb} = (\epsilon_a - \epsilon_i)\delta_{ij}\delta_{ab} + \langle ib|aj \rangle \tag{7a}$$

$$B_{ia,jb} = \langle ij|ab \rangle \tag{7b}$$

and where

$$\langle pq|rs \rangle = \iint \frac{\psi_p(\boldsymbol{x}_1)\psi_q(\boldsymbol{x}_2)\psi_r(\boldsymbol{x}_1)\psi_s(\boldsymbol{x}_2)}{|\boldsymbol{r}_1 - \boldsymbol{r}_2|} d\boldsymbol{x}_1 d\boldsymbol{x}_2 \tag{8}$$

is bare two-electron integrals in the spin−orbital basis.

The diagonal matrix $\boldsymbol{\Omega}$ contains the positive eigenvalues of the RPA problem defined in eq 6, and its elements Ω_{ν} appear in eq 4.

As mentioned above, because of the frequency dependence of the self-energy, solving exactly the quasiparticle eq 3 is a rather complicated task. Hence, several approximate schemes have

been developed to bypass full self-consistency. The most popular strategy is the one-shot (perturbative) GW scheme, G_0W_0, where the self-consistency is completely abandoned, and the off-diagonal elements of eq 3 are neglected. Assuming an HF starting point, this results in K quasiparticle equations that read

$$\epsilon_p^{\mathrm{HF}} + \Sigma_{pp}(\omega) - \omega = 0 \qquad (9)$$

where $\Sigma_{pp}(\omega)$ is the diagonal elements of $\boldsymbol{\Sigma}$, and ϵ_p^{HF} is the HF orbital energies. The previous equations are nonlinear with respect to ω and therefore have multiple solutions $\epsilon_{p,z}$ for a given p (where the index z is numbering solutions). These solutions can be characterized by their spectral weight given by the renormalization factor

$$0 \leq Z_{p,z} = \left[1 - \frac{\partial \Sigma_{pp}(\omega)}{\partial \omega} \bigg|_{\omega = \epsilon_{p,z}} \right]^{-1} \leq 1 \qquad (10)$$

The solution with the largest weight $Z_p \equiv Z_{p,z=0}$ is referred to as the quasiparticle, while the others are known as satellites (or shakeup transitions). However, in some cases, eq 9 can have two (or more) solutions with similar weights; hence, the quasiparticle is not well-defined.

One obvious drawback of the one-shot scheme mentioned above is its starting-point dependence. Indeed, in eq 9, we choose to rely on HF orbital energies, but this is arbitrary and one could have chosen Kohn–Sham energies (and orbitals) instead. As commonly done, one can even "tune" the starting point to obtain the best possible one-shot GW quasiparticle energies.[50,104,179−182]

Alternatively, one may solve iteratively the set of quasiparticle equations (eq 9) to reach convergence of the quasiparticle energies, leading to the partially self-consistent scheme named evGW. However, if one of the quasiparticle equations does not have a well-defined quasiparticle solution, reaching self-consistency can be challenging, if not impossible. Even at convergence, the starting point dependence is not totally removed as the quasiparticle energies still depend on the initial set of orbitals.[104]

In order to update both the orbitals and their corresponding energies, one must consider the off-diagonal elements in $\boldsymbol{\Sigma}(\omega)$. To avoid solving the non-Hermitian and dynamic quasiparticle equation defined in eq 3, one can resort to the qsGW scheme in which $\boldsymbol{\Sigma}(\omega)$ is replaced by a static approximation $\boldsymbol{\Sigma}^{\mathrm{qs}GW}$. Then, the qs$GW$ equations are solved via a standard self-consistent field procedure similar to the HF algorithm where $\boldsymbol{F}$ is replaced by $\boldsymbol{F} + \boldsymbol{\Sigma}^{\mathrm{qs}GW}$. Various choices for $\boldsymbol{\Sigma}^{\mathrm{qs}GW}$ are possible, but the most popular is the following Hermitian approximation

$$\Sigma_{pq}^{\mathrm{qs}GW} = \frac{1}{2}\mathrm{Re}[\Sigma_{pq}(\epsilon_p) + \Sigma_{pq}(\epsilon_q)] \qquad (11)$$

which was first introduced by Faleev and co-workers[107−109,183] before being derived by Ismail-Beigi as the effective Hamiltonian that minimizes the length of the gradient of the Klein functional for noninteracting Green's functions.[184] The corresponding matrix elements are

$$\Sigma_{pq}^{\mathrm{qs}GW} = \frac{1}{2} \sum_{r\nu} \left[\frac{\Delta_{pr}^\nu}{(\Delta_{pr}^\nu)^2 + \eta^2} + \frac{\Delta_{qr}^\nu}{(\Delta_{qr}^\nu)^2 + \eta^2} \right] W_{pr}^\nu W_{qr}^\nu \qquad (12)$$

with $\Delta_{pr}^\nu = \epsilon_p - \epsilon_r - \mathrm{sgn}(\epsilon_r - \epsilon_F)\Omega_\nu$ (where ϵ_F is the energy of the Fermi level). One of the main results of the present manuscript is

the derivation, from first-principles, of an alternative static Hermitian form for the qsGW self-energy.

Once again, in cases where multiple solutions have large spectral weights, self-consistency can be difficult to reach at the qsGW level. Multiple solutions of eq 9 arise due to the ω dependence of the self-energy. Therefore, by suppressing this dependence, the static approximation relies on the fact that there are well-defined quasiparticle solutions. If it is not the case, the self-consistent qsGW scheme inevitably oscillates between solutions with large spectral weights.[55]

The satellites causing convergence issues are the above-mentioned intruder states.[101] One can deal with them by introducing *ad hoc* regularizers. For example, the iη term in the denominators of eq 4, sometimes referred to as a broadening parameter linked to the width of the quasiparticle peak, is similar to the usual imaginary-shift regularizer employed in various other theories plagued by the intruder-state problem.[97,101,124,185]

However, this η parameter is required to define the Fourier transformation between time and energy representation and should theoretically be set to zero.[3] Several other regularizers are possible,[120−122,125,186,187] and in particular, it was shown in ref 101 that a regularizer inspired by the SRG had some advantages over the imaginary shift. Nonetheless, it would be more rigorous, and more instructive, to obtain this regularizer from first-principles by applying the SRG formalism to many-body perturbation theory. This is one of the aims of the present work.

III. THE SIMILARITY RENORMALIZATION GROUP

The SRG method aims at continuously transforming a general Hamiltonian matrix to its diagonal form or, more often, to a block-diagonal form. Hence, the first step is to decompose this Hamiltonian matrix

$$\boldsymbol{H} = \boldsymbol{H}^{\mathrm{d}} + \boldsymbol{H}^{\mathrm{od}} \qquad (13)$$

into an off-diagonal part, $\boldsymbol{H}^{\mathrm{od}}$, that we aim at removing and the remaining diagonal part, $\boldsymbol{H}^{\mathrm{d}}$.

This transformation can be performed continuously via a unitary matrix $\boldsymbol{U}(s)$, as follows

$$\boldsymbol{H}(s) = \boldsymbol{U}(s)\boldsymbol{H}\boldsymbol{U}^\dagger(s) \qquad (14)$$

where the flow parameter s controls the extent of the decoupling and is related to an energy cutoff $\Lambda = s^{-1/2}$. For a given value of s, only states with energy difference (with respect to the reference space) greater than Λ are decoupled from the reference space, hence avoiding potential intruders. By definition, the boundary conditions are $\boldsymbol{H}(s=0) = \boldsymbol{H}$ [or $\boldsymbol{U}(s=0) = \mathbf{1}$] and $\boldsymbol{H}^{\mathrm{od}}(s=\infty) = \boldsymbol{0}$.

An evolution equation for $\boldsymbol{H}(s)$ can be easily obtained by differentiating eq 14 with respect to s, yielding the flow equation

$$\frac{\mathrm{d}\boldsymbol{H}(s)}{\mathrm{d}s} = [\boldsymbol{\eta}(s), \boldsymbol{H}(s)] \qquad (15)$$

where $\boldsymbol{\eta}(s)$, the flow generator, is defined as

$$\boldsymbol{\eta}(s) = \frac{\mathrm{d}\boldsymbol{U}(s)}{\mathrm{d}s}\boldsymbol{U}^\dagger(s) = -\boldsymbol{\eta}^\dagger(s) \qquad (16)$$

The flow equation can then be approximately solved by introducing an approximate form of $\boldsymbol{\eta}(s)$.

In this work, we consider Wegner's canonical generator[126]

$$\boldsymbol{\eta}^{\mathrm{W}}(s) = [\boldsymbol{H}^{\mathrm{d}}(s), \boldsymbol{H}(s)] = [\boldsymbol{H}^{\mathrm{d}}(s)\boldsymbol{H}^{\mathrm{od}}(s)] \qquad (17)$$

which satisfies the following condition[188]

$$\frac{d}{ds}\text{Tr}[\boldsymbol{H}^{\text{od}}(s)^\dagger \boldsymbol{H}^{\text{od}}(s)] \leq 0 \tag{18}$$

This implies that the matrix elements of the off-diagonal part decrease in a monotonic way throughout the transformation. Moreover, the coupling coefficients associated with the highest-energy determinants are removed first as we shall evidence in the perturbative analysis below. The main drawback of this generator is that it generates a stiff set of ODE which is therefore difficult to solve numerically. However, here we will not tackle the full SRG problem but only consider analytical low-order perturbative expressions. Hence, we will not be affected by this problem.[142,189]

Let us now perform the perturbative analysis of the SRG equations. For $s = 0$, the initial problem is

$$\boldsymbol{H}(0) = \boldsymbol{H}^{\text{d}}(0) + \lambda \boldsymbol{H}^{\text{od}}(0) \tag{19}$$

where λ is the usual perturbation parameter, and the off-diagonal part of the Hamiltonian has been defined as the perturbation. For finite values of s, we have the following perturbation expansion of the Hamiltonian

$$\boldsymbol{H}(s) = \boldsymbol{H}^{(0)}(s) + \lambda \boldsymbol{H}^{(1)}(s) + \lambda^2 \boldsymbol{H}^{(2)}(s) + ... \tag{20}$$

The generator $\boldsymbol{\eta}(s)$ admits a similar perturbation expansion. Then, as performed in Sec. IV, one can collect order by order the terms in eq 15 and solve analytically the low-order differential equations.

IV. REGULARIZED *GW* APPROXIMATION

Here, we combine the concepts of the two previous subsections and apply the SRG method to the *GW* formalism. However, to do so, one must identify the coupling terms in eq 3, which is not straightforward. A way around this problem is to transform eq 3 to an equivalent upfolded form which elegantly highlights the coupling terms. Indeed, the *GW* quasiparticle equation is equivalent to the diagonalization of the following matrix[190,191]

$$\begin{pmatrix} \boldsymbol{F} & \boldsymbol{W}^{\text{2h1p}} & \boldsymbol{W}^{\text{2p1h}} \\ (\boldsymbol{W}^{\text{2h1p}})^\dagger & \boldsymbol{C}^{\text{2h1p}} & \boldsymbol{0} \\ (\boldsymbol{W}^{\text{2p1h}})^\dagger & \boldsymbol{0} & \boldsymbol{C}^{\text{2p1h}} \end{pmatrix} \tag{21}$$

where the 2h1p and 2p1h matrix elements are

$$C^{\text{2h1p}}_{i\nu,j\mu} = (\epsilon_i - \Omega_\nu)\delta_{ij}\delta_{\nu\mu} \tag{22a}$$

$$C^{\text{2p1h}}_{a\nu,b\mu} = (\epsilon_a + \Omega_\nu)\delta_{ab}\delta_{\nu\mu} \tag{22b}$$

and the corresponding coupling blocks read [see eq 5]

$$W^{\text{2h1p}}_{p,i\nu} = W^\nu_{pi}, \qquad W^{\text{2p1h}}_{p,a\nu} = W^\nu_{pa} \tag{23}$$

The usual *GW* nonlinear equation can be obtained by applying the Löwdin partitioning technique[192] to eq 21 yielding[190]

$$\boldsymbol{\Sigma}(\omega) = \boldsymbol{W}^{\text{2h1p}}(\omega\mathbf{1} - \boldsymbol{C}^{\text{2h1p}})^{-1}(\boldsymbol{W}^{\text{2h1p}})^\dagger$$
$$+ \boldsymbol{W}^{\text{2p1h}}(\omega\mathbf{1} - \boldsymbol{C}^{\text{2p1h}})^{-1}(\boldsymbol{W}^{\text{2p1h}})^\dagger \tag{24}$$

which can be further developed to recover exactly eq 4.

Equations 21 and 3 yield exactly the same quasiparticle and satellite energies, but one is linear and the other is not. The price to pay for this linearity is that the size of the matrix in the former

is $O(K^3)$, while it is only $O(K)$ in the latter. We refer to ref 190 for a detailed discussion of the up/downfolding processes of the *GW* equations (see also refs 191 and 119).

As can be readily seen in eq 21, the blocks $\boldsymbol{W}^{\text{2h1p}}$ and $\boldsymbol{W}^{\text{2p1h}}$ are coupling the 1h and 1p configurations to the 2h1p and 2p1h configurations. Therefore, it is natural to define, within the SRG formalism, the diagonal and off-diagonal parts of the *GW* effective Hamiltonian as

$$\boldsymbol{H}^{\text{d}}(s) = \begin{pmatrix} \boldsymbol{F} & \boldsymbol{0} & \boldsymbol{0} \\ \boldsymbol{0} & \boldsymbol{C}^{\text{2h1p}} & \boldsymbol{0} \\ \boldsymbol{0} & \boldsymbol{0} & \boldsymbol{C}^{\text{2p1h}} \end{pmatrix} \tag{25a}$$

$$\boldsymbol{H}^{\text{od}}(s) = \begin{pmatrix} \boldsymbol{0} & \boldsymbol{W}^{\text{2h1p}} & \boldsymbol{W}^{\text{2p1h}} \\ (\boldsymbol{W}^{\text{2h1p}})^\dagger & \boldsymbol{0} & \boldsymbol{0} \\ (\boldsymbol{W}^{\text{2p1h}})^\dagger & \boldsymbol{0} & \boldsymbol{0} \end{pmatrix} \tag{25b}$$

where we omit the s dependence of the matrices for the sake of brevity. Then, our aim is to solve, order by order, the flow equation (eq 15) knowing that the initial conditions are

$$\boldsymbol{H}^{(0)}_{\text{d}}(0) = \begin{pmatrix} \boldsymbol{F} & \boldsymbol{0} \\ \boldsymbol{0} & \boldsymbol{C} \end{pmatrix}, \qquad \boldsymbol{H}^{(0)}_{\text{od}}(0) = \boldsymbol{0} \tag{26a}$$

$$\boldsymbol{H}^{(1)}_{\text{d}}(0) = \boldsymbol{0}, \qquad \boldsymbol{H}^{(1)}_{\text{od}}(0) = \begin{pmatrix} \boldsymbol{0} & \boldsymbol{W} \\ \boldsymbol{W}^\dagger & \boldsymbol{0} \end{pmatrix} \tag{26b}$$

where the supermatrices

$$\boldsymbol{C} = \begin{pmatrix} \boldsymbol{C}^{\text{2h1p}} & \boldsymbol{0} \\ \boldsymbol{0} & \boldsymbol{C}^{\text{2p1h}} \end{pmatrix} \tag{27a}$$

$$\boldsymbol{W} = \begin{pmatrix} \boldsymbol{W}^{\text{2h1p}} & \boldsymbol{W}^{\text{2p1h}} \end{pmatrix} \tag{27b}$$

collect the 2h1p and 2p1h channels. Once the closed-form expressions of the low-order perturbative expansions are known, they can be inserted in eq 24 to define a renormalized version of the quasiparticle equation. In particular, we focus here on the second-order renormalized quasiparticle equation.

IV.A. Zeroth-Order Matrix Elements. The choice of Wegner's generator in the flow equation [see eq 15] implies that the off-diagonal correction is of order $O(\lambda)$ while the correction to the diagonal block is at least $O(\lambda^2)$.[142] Therefore, the zeroth-order Hamiltonian is independent of s, and we have

$$\boldsymbol{H}^{(0)}(s) = \boldsymbol{H}^{(0)}(0) \tag{28}$$

IV.B. First-Order Matrix Elements. Knowing that $\boldsymbol{H}^{(0)}_{\text{od}}(s) = \boldsymbol{0}$, the first-order flow equation is

$$\frac{d\boldsymbol{H}^{(1)}}{ds} = [[\boldsymbol{H}^{(0)}_{\text{d}}, \boldsymbol{H}^{(1)}_{\text{od}}], \boldsymbol{H}^{(0)}_{\text{d}}] \tag{29}$$

which gives the following system of equations

$$\frac{d\boldsymbol{F}^{(0)}}{ds} = \boldsymbol{0}, \qquad \frac{d\boldsymbol{C}^{(0)}}{ds} = \boldsymbol{0} \tag{30}$$

and

$$\frac{d\boldsymbol{W}^{(1)}}{ds} = 2\boldsymbol{F}^{(0)}\boldsymbol{W}^{(1)}\boldsymbol{C}^{(0)} - (\boldsymbol{F}^{(0)})^2\boldsymbol{W}^{(1)} - \boldsymbol{W}^{(1)}(\boldsymbol{C}^{(0)})^2 \tag{31}$$

Equation 30 implies

$$\boldsymbol{F}^{(1)}(s) = \boldsymbol{F}^{(1)}(0) = \boldsymbol{0} \tag{32a}$$

$$\boldsymbol{C}^{(1)}(s) = \boldsymbol{C}^{(1)}(0) = \boldsymbol{0} \tag{32b}$$

and thanks to the diagonal structure of $\boldsymbol{F}^0$ (which is a consequence of the HF starting point) and $\boldsymbol{C}^0$, the differential equation for the coupling block in eq 31 is easily solved and yields

$$W_{pq}^{\nu(1)}(s) = W_{pq}^{\nu} e^{-(\Delta_{pq}^{\nu})^2 s} \tag{33}$$

At $s = 0$, $W_{pq}^{\nu(1)}(s)$ reduces to the screened two-electron integrals defined in eq 5, while

$$\lim_{s \to \infty} W_{pq}^{\nu(1)}(s) = 0 \tag{34}$$

Therefore, $W_{pq}^{\nu(1)}(s)$ is a genuine renormalized two-electron screened integral. It is worth noting the close similarity of the first-order elements with the ones derived by Evangelista in ref 122 in the context of single- and multireference perturbation theory (see also ref 142).

IV.C. Second-Order Matrix Elements. The second-order renormalized quasiparticle equation is given by

$$[\tilde{\boldsymbol{F}}(s) + \tilde{\boldsymbol{\Sigma}}(\omega = \epsilon_p; s)]\psi_p(\boldsymbol{x}) = \epsilon_p \psi_p(\boldsymbol{x}) \tag{35}$$

with a renormalized Fock matrix of the form

$$\tilde{\boldsymbol{F}}(s) = \boldsymbol{F}^{(0)} + \boldsymbol{F}^{(2)}(s) \tag{36}$$

and a renormalized dynamical self-energy

$$\tilde{\boldsymbol{\Sigma}}(\omega; s) = \boldsymbol{V}^{(1)}(s)(\omega \boldsymbol{1} - \boldsymbol{C}^{(0)})^{-1}(\boldsymbol{V}^{(1)}(s))^{\dagger} \tag{37}$$

with elements

$$\tilde{\Sigma}_{pq}(\omega; s) = \sum_{i\nu} \frac{W_{pi}^{\nu} W_{qi}^{\nu}}{\omega - \epsilon_i + \Omega_\nu} e^{-[(\Delta_{pi}^{\nu})^2 + (\Delta_{qi}^{\nu})^2]s}$$
$$+ \sum_{a\nu} \frac{W_{pa}^{\nu} W_{qa}^{\nu}}{\omega - \epsilon_a - \Omega_\nu} e^{-[(\Delta_{pa}^{\nu})^2 + (\Delta_{qa}^{\nu})^2]s} \tag{38}$$

As can be readily seen above, $\boldsymbol{F}^{(2)}$ is the only second-order block of the effective Hamiltonian contributing to the second-order SRG quasiparticle equation. Collecting every second-order term in the flow equation and performing the block matrix products results in the following differential equation

$$\frac{d\boldsymbol{F}^{(2)}}{ds} = \boldsymbol{F}^{(0)} \boldsymbol{W}^{(1)} \boldsymbol{W}^{(1),\dagger} + \boldsymbol{W}^{(1)} \boldsymbol{W}^{(1),\dagger} \boldsymbol{F}^{(0)} - 2\boldsymbol{W}^{(1)} \boldsymbol{C}^{(0)} \boldsymbol{W}^{(1),\dagger} \tag{39}$$

which can be solved by simple integration along with the initial condition $\boldsymbol{F}^{(2)}(0) = \boldsymbol{0}$ to yield

$$F_{pq}^{(2)}(s) = \sum_{r\nu} \frac{\Delta_{pr}^{\nu} + \Delta_{qr}^{\nu}}{(\Delta_{pr}^{\nu})^2 + (\Delta_{qr}^{\nu})^2} W_{pr}^{\nu} W_{qr}^{\nu} [1 - e^{-[(\Delta_{pr}^{\nu})^2 + (\Delta_{qr}^{\nu})^2]s}] \tag{40}$$

At $s = 0$, the second-order correction vanishes, hence giving

$$\lim_{s \to 0} \tilde{\boldsymbol{F}}(s) = \boldsymbol{F}^{(0)} \tag{41}$$

For $s \to \infty$, it tends toward the following static limit

$$\lim_{s \to \infty} \tilde{\boldsymbol{F}}(s) = \epsilon_p \delta_{pq} + \sum_{r\nu} \frac{\Delta_{pr}^{\nu} + \Delta_{qr}^{\nu}}{(\Delta_{pr}^{\nu})^2 + (\Delta_{qr}^{\nu})^2} W_{pr}^{\nu} W_{qr}^{\nu} \tag{42}$$

while the dynamic part of the self-energy [see eq 37] tends to zero, i.e.,

$$\lim_{s \to \infty} \tilde{\boldsymbol{\Sigma}}(\omega; s) = \boldsymbol{0} \tag{43}$$

Therefore, the SRG flow continuously transforms the dynamical self-energy $\tilde{\boldsymbol{\Sigma}}(\omega; s)$ into a static correction $\tilde{\boldsymbol{F}}^{(2)}(s)$. As illustrated in Figure 1 (magenta curve), this transformation is done gradually starting from the states that have the largest denominators in eq 42.
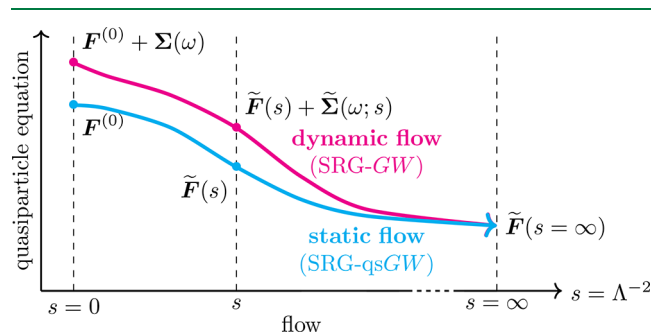
Figure 1. Schematic evolution of the quasiparticle equation as a function of the flow parameter s in the case of the dynamic SRG-GW flow (magenta) and the static SRG-qsGW flow (cyan).

For a fixed value of the energy cutoff Λ, if $|\Delta_{pr}^{\nu}| \gg \Lambda$, then $W_{pr}^{\nu} e^{-(\Delta_{pr}^{\nu})^2 s} \approx 0$, meaning that the state is decoupled from the 1h and 1p configurations, while for $|\Delta_{pr}^{\nu}| \ll \Lambda$, we have $W_{pr}^{\nu}(s) \approx W_{pr}^{\nu}$, that is, the state remains coupled.
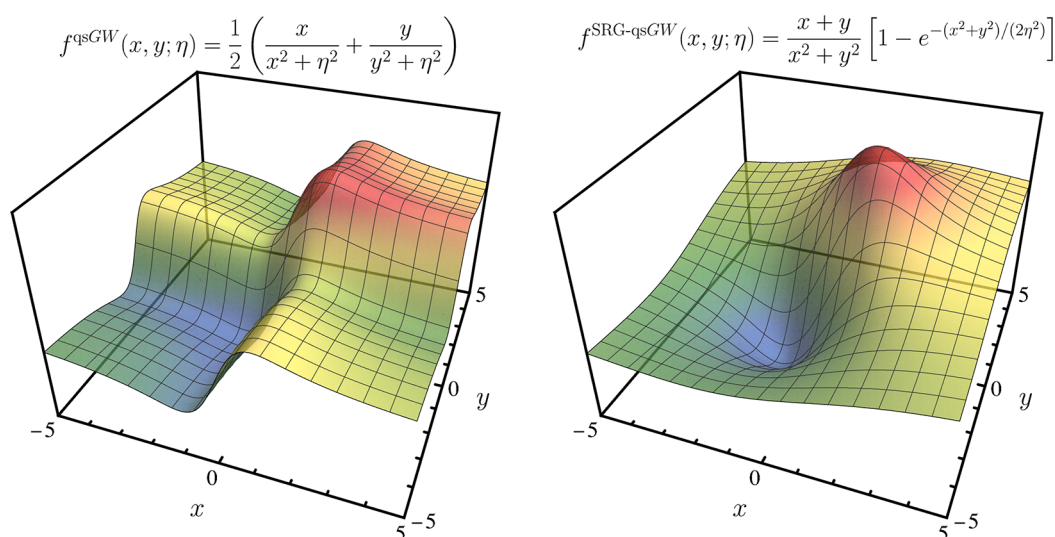
IV.D. Alternative Form of the Static Self-Energy. Because the large-s limit of eq 35 is purely static and Hermitian, the new alternative form of the self-energy reported in eq 42 can be naturally used in qsGW calculations to replace eq 11. Unfortunately, as we shall discuss further in Sec. VI, as $s \to \infty$, self-consistency is once again quite difficult to achieve, if not impossible. However, one can define a more flexible new static self-energy, which will be referred to as SRG-qsGW in the following, by discarding the dynamic part in eq 35 (see cyan curve in Figure 1). This yields an s-dependent static self-energy which matrix elements read

$$\Sigma_{pq}^{\text{SRG-qs}GW}(s) = \sum_{r\nu} \frac{\Delta_{pr}^{\nu} + \Delta_{qr}^{\nu}}{(\Delta_{pr}^{\nu})^2 + (\Delta_{qr}^{\nu})^2} W_{pr}^{\nu} W_{qr}^{\nu} [1 - e^{-[(\Delta_{pr}^{\nu})^2 + (\Delta_{qr}^{\nu})^2]s}] \tag{44}$$

Note that the static SRG-qsGW approximation defined in eq 44 is straightforward to implement in existing code and naturally Hermitian as opposed to the usual case [see eq 12] where it is enforced by brute-force symmetrization. Another important difference is that the SRG regularizer is energy-dependent, while the imaginary shift is the same for every self-energy denominator. Yet, these approximations are closely related because, for $\eta = 0$ and $s \to \infty$, they share the same diagonal terms.

It is well-known that in traditional qsGW calculations, increasing η to ensure convergence in difficult cases is most often unavoidable. Similarly, in SRG-qsGW, one might need to decrease the value of s to ensure convergence. Indeed, the fact that SRG-qsGW calculations do not always converge in the large-s limit is expected as, in this limit, potential intruder states have been included. Therefore, one should use a value of s large enough to include as many states as possible but small enough to avoid intruder states.

Journal of Chemical Theory and Computation
pubs.acs.org/JCTC
Article

$$f^{\mathrm{qs}GW}(x, y; \eta) = \frac{1}{2}\left(\frac{x}{x^2 + \eta^2} + \frac{y}{y^2 + \eta^2}\right)$$

$$f^{\mathrm{SRG\text{-}qs}GW}(x, y; \eta) = \frac{x + y}{x^2 + y^2}\left[1 - e^{-(x^2+y^2)/(2\eta^2)}\right]$$

Figure 2. Functional form of the qsGW self-energy (left) for $\eta = 1$ and the SRG-qsGW self-energy (right) for $s = 1/(2\eta^2) = 1/2$.

It is instructive to examine the functional form of both regularizing functions (see Figure 2). These have been plotted for a regularizing parameter value of $\eta = 1$, where we have set $s = 1/(2\eta^2)$ such that the first-order Taylor expansion around $(x, y) = (0, 0)$ of both functional forms is equal. One can observe that the SRG-qsGW surface is much smoother than its qsGW counterpart. This is due to the fact that the SRG-qsGW functional at $\eta = 0$, $f^{\mathrm{SRG\text{-}qs}GW}(x, y; 0)$, has fewer irregularities. In fact, there is a single singularity at $x = y = 0$. On the other hand, the function $f^{\mathrm{qs}GW}(x, y; 0)$ is singular on the two entire axes, $x = 0$ and $y = 0$. We believe that the smoothness of the SRG-qsGW surface is the key feature that explains the faster convergence of SRG-qsGW compared to qsGW. The convergence properties and the accuracy of both static approximations are quantitatively gauged in Sec. VI.

To conclude this section, we briefly discuss the case of discontinuities mentioned in Sec. I. Indeed, it has been previously mentioned that intruder states are responsible for both the poor convergence of qsGW and discontinuities in physical quantities.[44,100,101,116−119] Is it then possible to rely on the SRG machinery to remove discontinuities? Not directly because discontinuities are due to intruder states in the dynamic part of the quasiparticle equation. However, as we have seen just above the functional form of the renormalized equation makes it possible to choose s such that there are no intruder states in its static part. Performing a bijective transformation of the form

$$e^{-\Delta s} = 1 - e^{-\Delta t} \tag{45}$$

on the renormalized quasiparticle eq 35 reverses the situation and makes it possible to choose t such that there are no intruder states in the dynamic part, hence removing discontinuities. Note that, after this transformation, the form of the regularizer is actually closely related to the SRG-inspired regularizer introduced by Monino and Loos in ref 101.

The intruder-state-free dynamic part of the self-energy makes it possible to define SRG-G_0W_0 and SRG-evGW schemes. Although the manuscript focuses on SRG-qsGW, the performance of SRG-G_0W_0 and SRG-evGW are discussed in the Supporting Information for the sake of completeness. In a nutshell, the SRG regularization improves slightly the overall convergence properties of SRG-evGW without altering its

performance. Likewise, the statistical indicators for G_0W_0 and SRG-G_0W_0 are extremely close.

V. COMPUTATIONAL DETAILS

Our set of systems is composed by closed-shell compounds that correspond to the 50 smallest atoms and molecules (in terms of the number of electrons) of the GW100 benchmark set.[48] We will refer to this set as GW50. Following the same philosophy as the QUEST database for neutral excited states,[193,194] their geometries have been optimized at the CC3/aug-cc-pVTZ basis level[195,196] using the CFOUR program.[197] The optimized geometries are available in the Supporting Information.

The two qsGW variants considered in this work have been implemented in an in-house program, named QUACK.[198] The GW implementation closely follows the one of MOLGW.[178] In all GW calculations, we use the aug-cc-pVTZ Cartesian basis set, and self-consistency is performed on all (occupied and virtual) orbitals, including core orbitals. We use (restricted) HF guess orbitals and energies for all self-consistent GW calculations. The maximum size of the DIIS space[199,200] and the maximum number of iterations were set to 5 and 64, respectively. In practice, one may achieve convergence, in some cases, by adjusting these parameters or by using an alternative mixing scheme. However, in order to perform black-box comparisons, these parameters have been fixed to these default values. The η value has been set to 10^{-3} for the conventional G_0W_0 calculations (where we eschew linearizing the quasiparticle equation), while for the qsGW calculations, η has been chosen as the largest value where one successfully converges the 50 systems composing the test set.

The various GW-based sets of values are compared with a set of reference values computed at the ΔCCSD(T) level with the same basis set. The ΔCCSD(T) principal ionization potentials (IPs) and electron affinities (EAs) have been obtained using GAUSSIAN 16[201] (with default parameters) within the restricted and unrestricted formalism for the neutral and charged species, respectively.

VI. RESULTS

VI.A. Flow Parameter Dependence of SRG-qsGW. This section starts by considering a prototypical molecular system, the water molecule, in the aug-cc-pVTZ basis set. Figure 3 shows
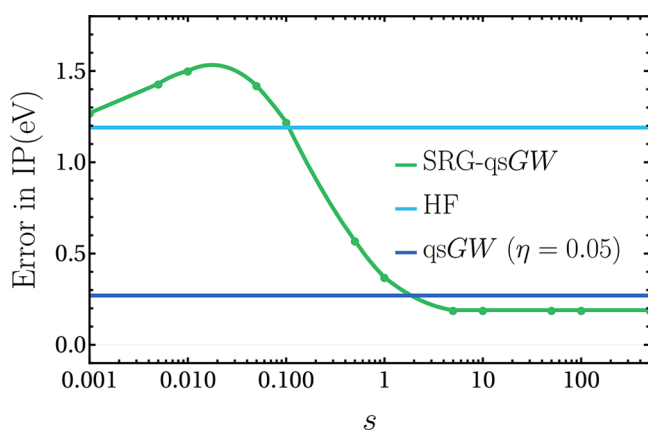
Figure 3. Error [with respect to ΔCCSD(T)] in the principal IP of water in the aug-cc-pVTZ basis set as a function of the flow parameter s for SRG-qsGW (green curve). The HF (cyan line) and qsGW (blue line) values are also reported.

the error in the principal IP [with respect to the ΔCCSD(T) reference value] as a function of the flow parameter in SRG-qsGW (green curve). The corresponding HF and qsGW (computed with $\eta = 0.05$) values are also reported for the sake of comparison. The IP at the HF level (cyan line) is too large; this is a consequence of the missing correlation and the lack of orbital relaxation in the cation, a result that is well understood.[93,148] The usual qsGW scheme (blue line) brings a quantitative improvement as the IP is now within 0.3 eV of the reference value.

At $s = 0$, the SRG-qsGW IP is equal to its HF counterpart as expected from the discussion of Sec. IV. As s grows, the IP reaches a plateau at an error that is significantly smaller than the HF starting point. Furthermore, the value associated with this plateau is slightly more accurate than its qsGW counterpart. However, the SRG-qsGW error does not decrease smoothly between the initial HF value and the large-s limit. For small s, it is actually worse than the HF starting point.

This behavior as a function of s can be understood by applying matrix perturbation theory to eq 21.[202] Through second order in the coupling block, the principal IP is

$$IP \approx -\epsilon_{\mathrm{h}} - \sum_{i\nu} \frac{(W^{\nu}_{\mathrm{h}i})^2}{\epsilon_{\mathrm{h}} - \epsilon_i + \Omega_{\nu}} - \sum_{a\nu} \frac{(W^{\nu}_{\mathrm{h}a})^2}{\epsilon_{\mathrm{h}} - \epsilon_a - \Omega_{\nu}} \tag{46}$$

where h is the index of the highest occupied molecular orbital (HOMO). The first term of the right-hand side of eq 46 is the zeroth-order IP, and the following two terms originate from the

2h1p and 2p1h coupling, respectively. The denominators of the 2p1h term are positive, while the denominators associated with the 2h1p term are negative.

As s increases, the first states that decouple from the HOMO are the 2p1h configurations because their energy difference with respect to the HOMO is larger than the ones associated with the 2h1p block. Therefore, for small s, only the last term of eq 46 is partially included, resulting in a positive correction to the IP. As soon as s is large enough to decouple the 2h1p block, the IP starts decreasing and eventually goes below the initial value at $s = 0$, as observed in Figure 3.

Next, the flow parameter dependence of SRG-qsGW is investigated for the principal IP of two additional molecular systems as well as the principal EA of F_2. The left panel of Figure 4 shows the results for the lithium dimer, Li_2, which is an interesting case because, unlike in water, HF underestimates the reference IP. Yet, the qsGW and SRG-qsGW IPs are still overestimating the reference value as in H_2O. Indeed, we can see that the positive increase of the SRG-qsGW IP is proportionally more important than for water. In addition, the plateau is reached for larger values of s in comparison to Figure 3.

Now turning to lithium hydride, LiH (see the middle panel of Figure 4), we see that the qsGW IP is actually worse than the fairly accurate HF value. However, SRG-qsGW does not suffer from the same problem and improves slightly the accuracy as compared to HF.

Finally, we also consider the evolution with respect to s of the principal EA of F_2 that is displayed in the right panel of Figure 4. The HF value is largely underestimating the ΔCCSD(T) reference. Performing a qsGW calculation on top of it brings a quantitative improvement by reducing the error from -2.03 eV to -0.24 eV. The SRG-qsGW EA (absolute) error is monotonically decreasing from the HF value at $s = 0$ to an error close to the qsGW one at $s \to \infty$.

VI.B. Statistical Analysis. Table I shows the principal IP of the 50 molecules considered in this work computed at various levels of theory. As previously mentioned, the HF approximation overestimates the IPs with a mean signed error (MSE) of 0.56 eV and a mean absolute error (MAE) of 0.69 eV. Performing a G_0W_0 calculation on top of this mean-field starting point, G_0W_0@HF, reduces by more than a factor of two the MSE and MAE, 0.29 and 0.33 eV, respectively. However, there are still outliers with large errors. For example, the IP of N_2 is overestimated by 1.56 eV, a large discrepancy that is due to the HF starting point. Self-consistency mitigates the error of the outliers as the MAE at the qsGW level is now 0.57 eV and the standard deviation of the error (SDE) is decreased from 0.31 eV for G_0W_0@HF to 0.18 eV for qsGW. In addition, the MSE and
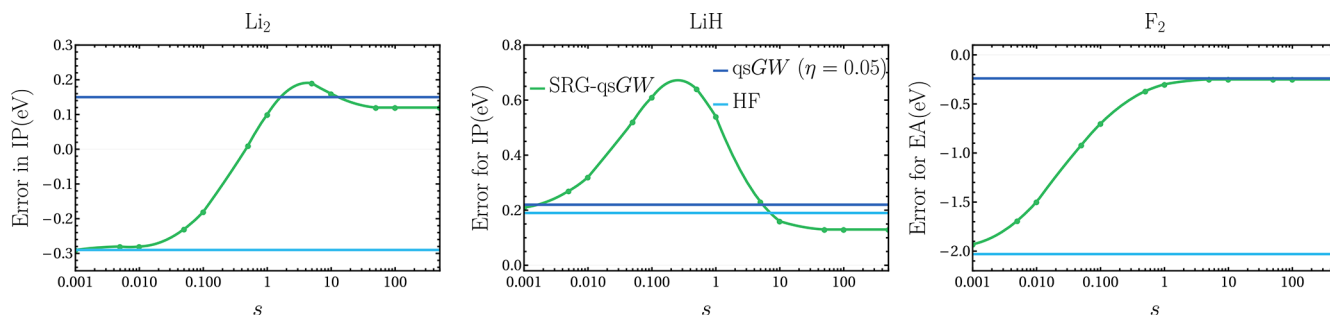

Figure 4. Error [with respect to ΔCCSD(T)] in the principal IP of Li_2, LiH, and the principal EA of F_2 in the aug-cc-pVTZ basis set as a function of the flow parameter s for the SRG-qsGW method (green curves). The HF (cyan lines) and qsGW (blue lines) values are also reported.

Table I. Principal IP and EA (in eV) of the *GW*50 Test Set Calculated Using ΔCCSD(T) (Reference), HF, G_0W_0@HF, qs*GW*, and SRG-qs*GW*[a]

	Principal IP					Principal EA				
Mol	ΔCCSD(T) (ref)	HF	G_0W_0@HF ($\eta = 10^{-3}$)	qs*GW* ($\eta = 10^{-1}$)	SRG-qs*GW* ($s = 10^3$)	ΔCCSD(T) (ref)	HF	G_0W_0@HF ($\eta = 10^{-3}$)	qs*GW* ($\eta = 10^{-1}$)	SRG-qs*GW* ($s = 10^3$)
He	24.54	24.98	24.59	24.58	24.55	−2.66	−2.70	−2.66	−2.66	−2.66
Ne	21.47	23.15	21.46	21.83	21.59	−5.09	−5.47	−5.25	−5.19	−5.19
H_2	16.40	16.16	16.49	16.45	16.45	−1.35	−1.33	−1.28	−1.28	−1.28
Li_2	5.25	4.96	5.38	5.40	5.37	0.34	−0.08	0.17	0.18	0.21
LiH	8.02	8.21	8.22	8.25	8.15	−0.29	0.20	0.27	0.27	0.27
HF	16.15	17.69	16.25	16.45	16.34	−0.66	−0.81	−0.71	−0.70	−0.70
Ar	15.60	16.08	15.72	15.61	15.63	−2.55	−2.97	−2.68	−2.64	−2.65
H_2O	12.69	13.88	12.90	12.98	12.88	−0.61	−0.80	−0.68	−0.65	−0.66
LiF	11.47	12.91	11.40	11.75	11.58	0.35	0.29	0.33	0.33	0.33
HCl	12.67	12.98	12.78	12.77	12.72	−0.57	−0.79	−0.64	−0.63	−0.63
BeO	9.95	10.45	9.74	10.32	10.18	2.17	1.80	2.28	2.10	2.13
CO	13.99	15.11	14.80	14.34	14.33	−1.57	−1.80	−1.66	−1.61	−1.62
N_2	15.54	16.68	17.10	15.93	15.91	−2.37	−2.20	−2.10	−2.10	−2.10
CH_4	14.39	14.83	14.76	14.67	14.63	−0.65	−0.79	−0.70	−0.68	−0.68
BH_3	13.31	13.59	13.68	13.62	13.59	−0.09	−0.81	−0.46	−0.29	−0.30
NH_3	10.91	11.69	11.22	11.18	11.10	−0.61	−0.80	−0.68	−0.66	−0.66
BF	11.15	11.04	11.34	11.19	11.18	−0.80	−1.06	−0.90	−0.87	−0.86
BN	12.05	11.55	11.76	11.89	11.90	3.02	2.97	3.90	3.41	3.44
SH_2	10.39	10.49	10.51	10.50	10.45	−0.52	−0.76	−0.60	−0.58	−0.59
F_2	15.81	18.15	16.35	16.27	16.22	0.32	−1.71	−0.53	0.10	0.07
MgO	7.97	8.75	8.40	8.54	8.36	1.54	1.40	1.64	1.72	1.71
O_3	12.85	13.29	13.56	13.34	13.27	1.82	1.32	2.19	2.23	2.17
C_2H_2	11.45	11.16	11.57	11.46	11.43	−0.80	−0.80	−0.71	−0.71	−0.71
HCN	13.76	13.50	13.86	13.75	13.73	−0.53	−0.61	−0.52	−0.55	−0.54
B_2H_6	12.27	12.84	12.81	12.67	12.64	−0.52	−0.64	−0.56	−0.55	−0.55
CH_2O	10.93	12.09	11.39	11.33	11.25	−0.60	−0.70	−0.61	−0.62	−0.62
C_2H_4	10.69	10.26	10.74	10.70	10.67	−1.90	−0.86	−0.75	−0.73	−0.74
SiH_4	12.79	13.23	13.22	13.15	13.11	−0.53	−0.69	−0.59	−0.57	−0.58
PH_3	10.60	10.60	10.79	10.76	10.73	−0.51	−0.71	−0.58	−0.56	−0.57
CH_4O	11.09	12.30	11.55	11.49	11.39	−0.59	−0.76	−0.64	−0.62	−0.63
H_2NNH_2	9.49	10.38	9.84	9.81	9.73	−0.60	−0.82	−0.69	−0.65	−0.65
HOOH	11.51	13.17	11.96	11.95	11.86	−0.96	−0.89	−0.75	−0.72	−0.72
KH	6.32	6.61	6.44	6.50	6.38	0.30	0.21	0.28	0.28	0.28
Na_2	4.93	4.53	4.98	5.03	5.01	0.36	−0.01	0.26	0.27	0.30
HN_3	10.77	11.00	11.12	10.92	10.89	−0.51	−0.75	−0.6	−0.56	−0.56
CO_2	13.80	14.82	14.24	14.12	14.06	−0.88	−1.22	−0.98	−0.95	−0.95
PN	11.90	12.00	12.33	12.12	12.09	−0.02	−0.72	−0.03	0.02	0.00
CH_2O_2	11.54	12.94	12.00	11.97	11.88	−0.63	−0.79	−0.69	−0.66	−0.67
C_4	11.43	11.61	11.77	11.57	11.54	2.38	0.58	2.24	2.29	2.30
C_3H_6	10.83	11.25	11.20	11.07	11.03	−0.94	−0.88	−0.75	−0.73	−0.73
C_2H_3F	10.63	10.48	10.84	10.73	10.69	−0.65	−0.80	−0.69	−0.68	−0.68
C_2H_4O	10.29	11.64	10.84	10.74	10.66	−0.54	−0.69	−0.56	−0.57	−0.57
C_2H_6O	10.82	12.05	11.37	11.25	11.15	−0.58	−0.78	−0.65	−0.62	−0.62
C_3H_8	12.13	12.73	12.61	12.51	12.46	−0.63	−0.83	−0.70	−0.67	−0.67
NaCl	9.10	9.60	9.20	9.25	9.16	0.67	0.56	0.64	0.64	0.64
P_2	10.72	10.05	10.49	10.43	10.40	0.43	−0.35	0.47	0.48	0.47
MgF_2	13.93	15.46	13.94	14.23	14.07	0.29	−0.03	0.15	0.21	0.21
OCS	11.23	11.44	11.52	11.37	11.32	−1.43	−1.27	−1.03	−0.97	−0.98
SO_2	10.48	11.47	11.38	10.85	10.82	2.24	1.84	2.82	2.74	2.68
C_2H_3Cl	10.17	10.13	10.39	10.27	10.24	−0.61	−0.79	−0.66	−0.65	−0.65
MSE		0.56	0.29	0.23	0.17		−0.25	0.02	0.04	0.04
MAE		0.69	0.33	0.25	0.19		0.31	0.16	0.13	0.12
RMSE		0.87	0.43	0.29	0.23		0.49	0.28	0.23	0.22
SDE		0.68	0.31	0.18	0.16		0.43	0.29	0.23	0.22
Min		−0.67	−0.29	−0.29	−0.32		−2.03	−0.85	−0.22	−0.25
Max		2.34	1.56	0.57	0.42		1.04	1.15	1.17	1.16

[a]The statistical descriptors associated with the errors with respect to the reference values are also reported. All calculations are performed with the aug-cc-pVTZ basis.
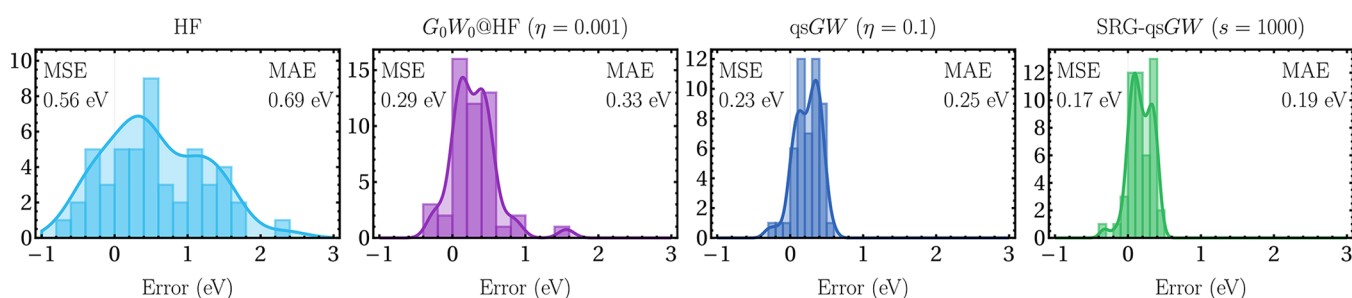
Figure 5. Histogram of the errors [with respect to $\Delta CCSD(T)$] for the principal IP of the GW50 test set calculated using HF, G_0W_0@HF, qsGW, and SRG-qsGW. All calculations are performed with the aug-cc-pVTZ basis.

MAE (0.23 and 0.25 eV, respectively) are also slightly improved with respect to G_0W_0@HF (see Figure 5).

Let us now turn to our new method, the SRG-qsGW self-consistent scheme. Table I shows the SRG-qsGW values for $s = 10^3$. The statistical descriptors corresponding to this alternative static self-energy are all improved with respect to qsGW. In particular, the MSE and MAE are decreased by 0.06 eV. Of course, these are small improvements; but this is done with no additional computational cost, and it can be easily implemented in existing code by changing the form of the static self-energy. The evolution of the statistical descriptors with respect to the various methods considered in Table I is graphically illustrated in Figure 4. The decrease of the MSE and SDE correspond to a shift of the maximum of the distribution toward zero and a contraction of the distribution width, respectively.

In addition to this improvement in terms of accuracy, the SRG-qsGW scheme has been found to be much easier to converge than its qsGW parent. Indeed, up to $s = 10^3$, it is straightforward to reach self-consistency for the 50 compounds at the SRG-qsGW level. For $s = 5 \times 10^3$, convergence could not be attained for 11 systems out of 50. However, this is not a serious issue as the MAE of the test set is already well converged at $s = 10^3$. This is illustrated by the green curve of Figure 6 which shows the evolution of the SRG-qsGW MAE with respect to s. The convergence plateau of the MAE is reached around $s = 50$, while the convergence problems arise for $s > 10^3$. Therefore, for
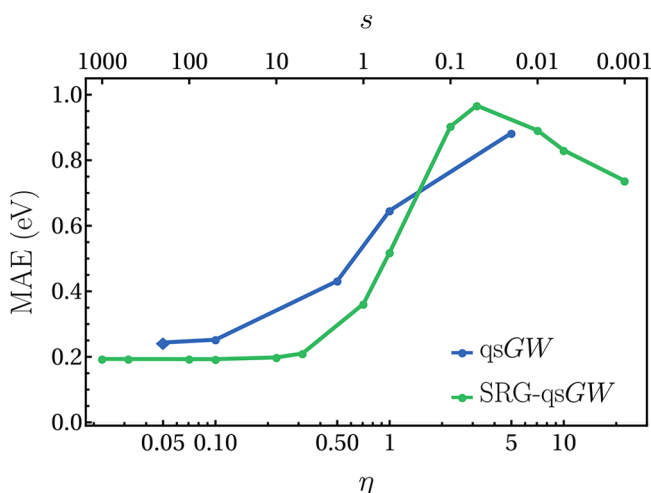
future studies using the SRG-qsGW method, a default value of the flow parameter equal to 5×10^2 or 10^3 is recommended.

On the other hand, the qsGW convergence behavior is more erratic as shown by the blue curve of Figure 6 where we report the variation of the qsGW MAE as a function of $\eta = \sqrt{1/(2s)}$. At $\eta = 10^{-2}$ ($s = 5 \times 10^3$), convergence could not be reached for 13 molecules, while 2 systems were already problematic at $\eta = 5 \times 10^{-2}$ ($s = 200$). These convergence problems are much more dramatic than for SRG-qsGW because the MAE has not reached its limiting value before these issues arise. For example, out of the 37 molecules that could be converged for $\eta = 10^{-2}$, the variation of the IP with respect to $\eta = 5 \times 10^{-2}$ can go up to 0.1 eV.
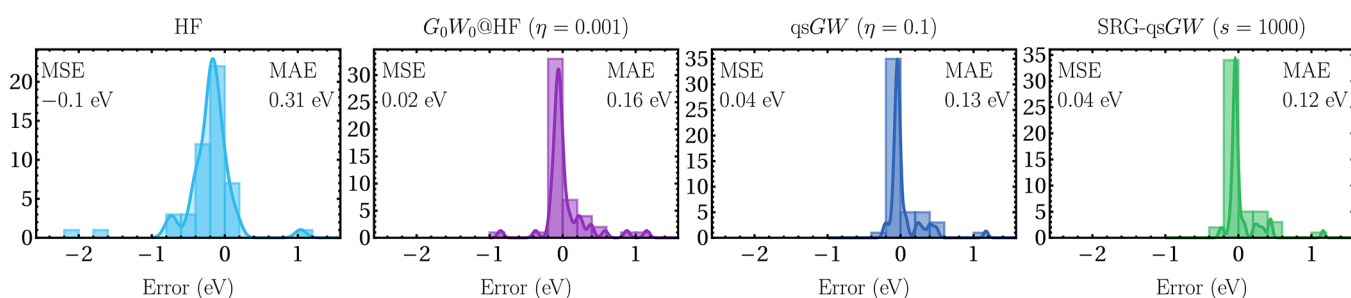
This difference in behavior is due to the energy (in)-dependence of the regularizers. The SRG regularizer first incorporates the terms with a large denominator and subsequently adds the intruder states. Conversely, the imaginary shift regularizer treats all terms equivalently.

Finally, we compare the performance of HF, G_0W_0@HF, qsGW, and SRG-qsGW again but for the principal EAs of GW50. The raw data are reported in Table I, while the corresponding histograms of the error distribution are plotted in Figure 7. The HF EAs are, on average, underestimated with an MAE of 0.31 eV and some clear outliers: -2.03 eV for F_2 and 1.04 eV for CH_2O, for example. G_0W_0@HF mitigates the average error (MAE equals to 0.16 eV), but the minimum and maximum error values are not satisfactory. The performance of the two qsGW schemes are quite similar for EAs with MAEs of the order of 0.1 eV. These two partially self-consistent methods reduce also the minimum errors, but interestingly, they do not decrease the maximum error compared to HF.

Note that a positive EA indicates a bounded anion state, which can be accurately described by the methods considered in this study. However, a negative EA suggests a resonance state, which is beyond the scope of the methods used in this study, including the $\Delta CCSD(T)$ reference. As such, it is not advisable to assign a physical interpretation to these values. Nonetheless, it is possible to compare GW-based and $\Delta CCSD(T)$ values in such cases, provided that the comparison is limited to a given basis set.

VII. CONCLUSION

The present manuscript applies the similarity renormalization group (SRG) to the GW approximation of many-body perturbation theory, which is known to be plagued by intruder states. The problems caused by intruder states in many-body perturbation theory are numerous, but here, we focus on the convergence issues caused by them.

Figure 6. Evolution of the SRG-qsGW (green) and qsGW (blue) MAEs for the principal IPs of the GW50 test set as functions of s and η, respectively. The bottom and top axes are related by $s = 1/(2\eta^2)$. A different marker has been used for qsGW at $\eta = 0.05$ because the MAE includes only 48 molecules.

Figure 7. Histogram of the errors [with respect to ΔCCSD(T)] for the principal EA of the GW50 test set calculated using HF, G_0W_0@HF, qsGW, and SRG-qsGW. All calculations are performed with the aug-cc-pVTZ basis.

SRG's central equation is the flow equation, which is usually solved numerically but can be solved analytically for low perturbation order. Applying this approach in the GW context yields closed-form renormalized expressions for the Fock matrix elements and the screened two-electron integrals. These renormalized quantities lead to a regularized GW quasiparticle equation, referred to as SRG-GW, which is the main result of this work.

By isolating the static component of SRG-GW, we obtain an alternative Hermitian and intruder-state-free self-energy that can be used in the context of qsGW calculations. This new variant is called SRG-qsGW. Additionally, we demonstrate how SRG-GW can effectively resolve the discontinuity problems that arise in GW due to intruder states. This provides a first-principles justification for the SRG-inspired regularizer proposed in ref 101.

We first study the flow parameter dependence of the SRG-qsGW IPs for a few test cases. The results show that the IPs gradually evolve from the HF starting point at $s = 0$ to a plateau value for $s \to \infty$ that is much closer to the ΔCCSD(T) reference than the HF initial value. For small values of the flow parameter, the SRG-qsGW IPs are actually worse than their starting point. Therefore, it is advisable to use the largest possible value of s, similar to qsGW calculations where one needs to use the smallest possible η value.

Next, we gauge the accuracy of the SRG-qsGW principal IP for a test set of 50 atoms and molecules (referred to as GW50). The results show that, on average, SRG-qsGW is slightly better than its qsGW parent. Despite the fact that the increase in accuracy is relatively modest, it comes with no additional computational cost and is straightforward to implement, as only the expression of the static self-energy needs to be modified. Moreover, SRG-qsGW calculations are much easier to converge than their traditional qsGW counterparts thanks to the intruder-state-free nature of SRG-qsGW.

Finally, the principal EAs of the GW50 set are also investigated. It is found that the performances of qsGW and SRG-qsGW are quite similar in this case. However, it should be noted that most of the anions of the GW50 set are resonance states, and the associated physics cannot be accurately described by the methods considered in this study. Therefore, test sets of molecules with bound anions, such as this one of organic electron-acceptor molecules,[182,203−205] and their accompanying accurate reference values are greatly valuable to the electronic structure community.

■ AUTHOR INFORMATION

Corresponding Authors

    Pierre-François Loos − *Laboratoire de Chimie et Physique Quantiques (UMR 5626), Université de Toulouse, CNRS, UPS, 31400 Toulouse, France;* ⓞ orcid.org/0000-0003-0598-7425; Email: loos@irsamc.ups-tlse.fr

    Antoine Marie − *Laboratoire de Chimie et Physique Quantiques (UMR 5626), Université de Toulouse, CNRS, UPS, 31400 Toulouse, France;* ⓞ orcid.org/0000-0003-3605-0176; Email: amarie@irsamc.ups-tlse.fr

Complete contact information is available at:
https://pubs.acs.org/10.1021/acs.jctc.3c00281

Notes

The authors declare no competing financial interest.

■ REFERENCES

(1) Csanak, G.; Taylor, H.; Yaris, R. Green's Function Technique in Atomic and Molecular Physics. *Advances in atomic and molecular physics*; Elsevier: 1971; Vol. 7, pp 287−361.

(2) Fetter, A. L.; Waleck, J. D. *Quantum Theory of Many Particle Systems*; McGraw Hill: San Francisco, 1971.

(3) Martin, R. M.; Reining, L.; Ceperley, D. M. *Interacting Electrons: Theory and Computational Approaches*; Cambridge University Press: 2016.

(4) Golze, D.; Dvorak, M.; Rinke, P. The GW Compendium: A Practical Guide to Theoretical Photoemission Spectroscopy. *Front. Chem.* **2019**, *7*, 377.

(5) Hedin, L. New Method for Calculating the One-Particle Green's Function with Application to the Electron-Gas Problem. *Phys. Rev.* **1965**, *139*, A796.

(6) Aryasetiawan, F.; Gunnarsson, O. The GW Method. *Rep. Prog. Phys.* **1998**, *61*, 237−312.

(7) Onida, G.; Reining, L.; Rubio, A. Electronic Excitations: Density-Functional Versus Many-Body Green's Function Approaches. *Rev. Mod. Phys.* **2002**, *74*, 601−659.

(8) Reining, L. The *GW* Approximation: Content, Successes and Limitations: The *GW* Approximation. *Wiley Interdiscip. Rev. Comput. Mol. Sci.* **2018**, *8*, e1344.

(9) Bruneval, F.; Dattani, N.; van Setten, M. J. The *GW* Miracle in Many-Body Perturbation Theory for the Ionization Potential of Molecules. *Front. Chem.* **2021**, *9*, 749779.

(10) Strinati, G.; Mattausch, H. J.; Hanke, W. Dynamical Correlation Effects on the Quasiparticle Bloch States of a Covalent Crystal. *Phys. Rev. Lett.* **1980**, *45*, 290−294.

(11) Strinati, G.; Mattausch, H. J.; Hanke, W. Dynamical Aspects of Correlation Corrections in a Covalent Crystal. *Phys. Rev. B* **1982**, *25*, 2867−2888.

(12) Strinati, G. Dynamical Shift and Broadening of Core Excitons in Semiconductors. *Phys. Rev. Lett.* **1982**, *49*, 1519.

(13) Hybertsen, M. S.; Louie, S. G. First-Principles Theory of Quasiparticles: Calculation of Band Gaps in Semiconductors and Insulators. *Phys. Rev. Lett.* **1985**, *55*, 1418.

(14) Hybertsen, M. S.; Louie, S. G. Electron Correlation in Semiconductors and Insulators: Band Gaps and Quasiparticle Energies. *Phys. Rev. B* **1986**, *34*, 5390−5413.

(15) Godby, R. W.; Schlüter, M.; Sham, L. J. Accurate Exchange-Correlation Potential for Silicon and Its Discontinuity on Addition of an Electron. *Phys. Rev. Lett.* **1986**, *56*, 2415−2418.

(16) Godby, R. W.; Schlüter, M.; Sham, L. J. Trends in Self-Energy Operators and Their Corresponding Exchange-Correlation Potentials. *Phys. Rev. B* **1987**, *36*, 6497−6500.

(17) Godby, R. W.; Schlüter, M.; Sham, L. J. Quasiparticle Energies in GaAs and AlAs. *Phys. Rev. B* **1987**, *35*, 4170−4171.

(18) Godby, R. W.; Schlüter, M.; Sham, L. J. Self-Energy Operators and Exchange-Correlation Potentials in Semiconductors. *Phys. Rev. B* **1988**, *37*, 10159−10175.

(19) Blase, X.; Rubio, A.; Louie, S. G.; Cohen, M. L. Quasiparticle Band Structure of Bulk Hexagonal Boron Nitride and Related Systems. *Phys. Rev. B* **1995**, *51*, 6868−6875.

(20) Rohlfing, M.; Louie, S. G. Optical Excitations in Conjugated Polymers. *Phys. Rev. Lett.* **1999**, *82*, 1959−1962.

(21) van der Horst, J.-W.; Bobbert, P. A.; Michels, M. A. J.; Brocks, G.; Kelly, P. J. Ab Initio Calculation of the Electronic and Optical Excitations in Polythiophene: Effects of Intra- and Interchain Screening. *Phys. Rev. Lett.* **1999**, *83*, 4413−4416.

(22) Puschnig, P.; Ambrosch-Draxl, C. Suppression of Electron-Hole Correlations in 3D Polymer Materials. *Phys. Rev. Lett.* **2002**, *89*, 056405.

(23) Tiago, M. L.; Northrup, J. E.; Louie, S. G. Ab Initio Calculation of the Electronic and Optical Properties of Solid Pentacene. *Phys. Rev. B* **2003**, *67*, 115212.

(24) Rocca, D.; Lu, D.; Galli, G. Ab Initio Calculations of Optical Absorption Spectra: Solution of the Bethe−Salpeter Equation Within Density Matrix Perturbation Theory. *J. Chem. Phys.* **2010**, *133*, 164109.

(25) Boulanger, P.; Jacquemin, D.; Duchemin, I.; Blase, X. Fast and Accurate Electronic Excitations in Cyanines with the Many-Body Bethe-Salpeter Approach. *J. Chem. Theory Comput.* **2014**, *10*, 1212−1218.

(26) Jacquemin, D.; Duchemin, I.; Blase, X. Benchmarking the Bethe−Salpeter Formalism on a Standard Organic Molecular Set. *J. Chem. Theory Comput.* **2015**, *11*, 3290−3304.

(27) Bruneval, F.; Hamed, S. M.; Neaton, J. B. A systematic benchmark of the ab initio Bethe-Salpeter equation approach for low-lying optical excitations of small organic molecules. *J. Chem. Phys.* **2015**, *142*, 244101.

(28) Jacquemin, D.; Duchemin, I.; Blase, X. 0−0 Energies Using Hybrid Schemes: Benchmarks of TD-DFT, CIS(D), ADC(2), CC2, and BSE/*GW* formalisms for 80 Real-Life Compounds. *J. Chem. Theory Comput.* **2015**, *11*, 5340−5359.

(29) Hirose, D.; Noguchi, Y.; Sugino, O. All-Electron GW+Bethe-Salpeter Calculations on Small Molecules. *Phys. Rev. B* **2015**, *91*, 205111.

(30) Jacquemin, D.; Duchemin, I.; Blase, X. Is the Bethe−Salpeter Formalism Accurate for Excitation Energies? Comparisons with TD-DFT, CASPT2, and EOM-CCSD. *J. Phys. Chem. Lett.* **2017**, *8*, 1524−1529.

(31) Jacquemin, D.; Duchemin, I.; Blondel, A.; Blase, X. Benchmark of Bethe-Salpeter for Triplet Excited-States. *J. Chem. Theory Comput.* **2017**, *13*, 767−783.

(32) Rangel, T.; Hamed, S. M.; Bruneval, F.; Neaton, J. B. An Assessment of Low-Lying Excitation Energies and Triplet Instabilities of Organic Molecules with an *Ab Initio* Bethe-Salpeter Equation Approach and the Tamm-Dancoff Approximation. *J. Chem. Phys.* **2017**, *146*, 194108.

(33) Krause, K.; Klopper, W. Implementation of the Bethe-Salpeter equation in the TURBOMOLE program. *J. Comput. Chem.* **2017**, *38*, 383−388.

(34) Gui, X.; Holzer, C.; Klopper, W. Accuracy Assessment of *GW* Starting Points for Calculating Molecular Excitation Energies Using the Bethe−Salpeter Formalism. *J. Chem. Theory Comput.* **2018**, *14*, 2127−2136.

(35) Blase, X.; Duchemin, I.; Jacquemin, D. The Bethe−Salpeter equation in chemistry: relations with TD-DFT, applications and challenges. *Chem. Soc. Rev.* **2018**, *47*, 1022−1043.

(36) Liu, C.; Kloppenburg, J.; Yao, Y.; Ren, X.; Appel, H.; Kanai, Y.; Blum, V. All-electron ab initio Bethe-Salpeter equation approach to neutral excitations in molecules with numeric atom-centered orbitals. *J. Chem. Phys.* **2020**, *152*, 044105.

(37) Li, J.; Holzmann, M.; Duchemin, I.; Blase, X.; Olevano, V. Helium Atom Excitations by the G W and Bethe-Salpeter Many-Body Formalism. *Phys. Rev. Lett.* **2017**, *118*, 163001.

(38) Li, J.; Drummond, N. D.; Schuck, P.; Olevano, V. Comparing Many-Body Approaches Against the Helium Atom Exact Solution. *SciPost Phys.* **2019**, *6*, 040.

(39) Li, J.; Duchemin, I.; Blase, X.; Olevano, V. Ground-state correlation energy of beryllium dimer by the Bethe-Salpeter equation. *SciPost Phys.* **2020**, *8*, 020.

(40) Li, J.; Olevano, V. Hydrogen-molecule spectrum by the many-body *GW* approximation and the Bethe-Salpeter equation. *Phys. Rev. A* **2021**, *103*, 012809.

(41) Blase, X.; Duchemin, I.; Jacquemin, D.; Loos, P.-F. The Bethe-Salpeter Equation Formalism: From Physics to Chemistry. *J. Phys. Chem. Lett.* **2020**, *11*, 7371−7382.

(42) Holzer, C.; Klopper, W. A hybrid Bethe−Salpeter/time-dependent density-functional-theory approach for excitation energies. *J. Chem. Phys.* **2018**, *149*, 101101.

(43) Holzer, C.; Gui, X.; Harding, M. E.; Kresse, G.; Helgaker, T.; Klopper, W. Bethe-Salpeter Correlation Energies of Atoms and Molecules. *J. Chem. Phys.* **2018**, *149*, 144106.

(44) Loos, P.-F.; Scemama, A.; Duchemin, I.; Jacquemin, D.; Blase, X. Pros and Cons of the Bethe−Salpeter Formalism for Ground-State Energies. *J. Phys. Chem. Lett.* **2020**, *11*, 3536−3545.

(45) Loos, P.-F.; Comin, M.; Blase, X.; Jacquemin, D. Reference Energies for Intramolecular Charge-Transfer Excitations. *J. Chem. Theory Comput.* **2021**, *17*, 3666−3686.

(46) McKeon, C. A.; Hamed, S. M.; Bruneval, F.; Neaton, J. B. An optimally tuned range-separated hybrid starting point for ab initio *GW* plus Bethe−Salpeter equation calculations of molecules. *J. Chem. Phys.* **2022**, *157*, 074103.

(47) Hung, L.; Bruneval, F.; Baishya, K.; Öğüt, S. Benchmarking the *GW* Approximation and Bethe−Salpeter Equation for Groups IB and IIB Atoms and Monoxides. *J. Chem. Theory Comput.* **2017**, *13*, 2135−2146.

(48) van Setten, M. J.; Caruso, F.; Sharifzadeh, S.; Ren, X.; Scheffler, M.; Liu, F.; Lischner, J.; Lin, L.; Deslippe, J. R.; Louie, S. G.; Yang, C.; Weigend, F.; Neaton, J. B.; Evers, F.; Rinke, P. *GW*100: Benchmarking G_0W_0 for Molecular Systems. *J. Chem. Theory Comput.* **2015**, *11*, 5665−5687.

(49) van Setten, M. J.; Costa, R.; Viñes, F.; Illas, F. Assessing *GW* Approaches for Predicting Core Level Binding Energies. *J. Chem. Theory Comput.* **2018**, *14*, 877−883.

(50) Caruso, F.; Dauth, M.; van Setten, M. J.; Rinke, P. Benchmark of *GW* Approaches for the *GW*100 Test Set. *J. Chem. Theory Comput.* **2016**, *12*, 5076.

(51) Körbel, S.; Boulanger, P.; Duchemin, I.; Blase, X.; Marques, M. A. L.; Botti, S. Benchmark Many-Body *GW* and Bethe−Salpeter Calculations for Small Transition Metal Molecules. *J. Chem. Theory Comput.* **2014**, *10*, 3934−3943.

(52) Foerster, D.; Koval, P.; Sánchez-Portal, D. An O(N3) implementation of Hedin's *GW* approximation for molecules. *J. Chem. Phys.* **2011**, *135*, 074105.

(53) Liu, P.; Kaltak, M.; Klimeš, J. c. v.; Kresse, G. Cubic Scaling *GW*: Towards Fast Quasiparticle Calculations. *Phys. Rev. B* **2016**, *94*, 165109.

(54) Wilhelm, J.; Golze, D.; Talirz, L.; Hutter, J.; Pignedoli, C. A. Toward *GW* Calculations on Thousands of Atoms. *J. Phys. Chem. Lett.* **2018**, *9*, 306−312.

(55) Förster, A.; Visscher, L. Low-Order Scaling Quasiparticle Self-Consistent *GW* for Molecules. *Front. Chem.* **2021**, *9*, 736591.

(56) Duchemin, I.; Blase, X. Separable resolution-of-the-identity with all-electron Gaussian bases: Application to cubic-scaling RPA. *J. Chem. Phys.* **2019**, *150*, 174120.

(57) Duchemin, I.; Blase, X. Robust Analytic-Continuation Approach to Many-Body *GW* Calculations. *J. Chem. Theory Comput.* **2020**, *16*, 1742−1756.

(58) Duchemin, I.; Blase, X. Cubic-Scaling All-Electron *GW* Calculations with a Separable Density-Fitting Space−Time Approach. *J. Chem. Theory Comput.* **2021**, *17*, 2383−2393.

(59) Ren, X.; Rinke, P.; Joas, C.; Scheffler, M. Random-Phase Approximation and Its Applications in Computational Chemistry and Materials Science. *J. Mater. Sci.* **2012**, *47*, 7447−7471.

(60) Chen, G. P.; Voora, V. K.; Agee, M. M.; Balasubramani, S. G.; Furche, F. Random-Phase Approximation Methods. *Annu. Rev. Phys. Chem.* **2017**, *68*, 421−445.

(61) Kozik, E.; Ferrero, M.; Georges, A. Nonexistence of the Luttinger-Ward Functional and Misleading Convergence of Skeleton Diagrammatic Series for Hubbard-Like Models. *Phys. Rev. Lett.* **2015**, *114*, 156402.

(62) Stan, A.; Romaniello, P.; Rigamonti, S.; Reining, L.; Berger, J. A. Unphysical and physical solutions in many-body theories: from weak to strong correlation. *New J. Phys.* **2015**, *17*, 093045.

(63) Rossi, R.; Werner, F. Skeleton series and multivaluedness of the self-energy functional in zero space-time dimensions. *J. Phys. A: Math. Theor.* **2015**, *48*, 485202.

(64) Tarantino, W.; Romaniello, P.; Berger, J. A.; Reining, L. Self-Consistent Dyson Equation and Self-Energy Functionals: An Analysis and Illustration on the Example of the Hubbard Atom. *Phys. Rev. B* **2017**, *96*, 045124.

(65) Schäfer, T.; Rohringer, G.; Gunnarsson, O.; Ciuchi, S.; Sangiovanni, G.; Toschi, A. Divergent Precursors of the Mott-Hubbard Transition at the Two-Particle Level. *Phys. Rev. Lett.* **2013**, *110*, 246405.

(66) Schäfer, T.; Ciuchi, S.; Wallerberger, M.; Thunström, P.; Gunnarsson, O.; Sangiovanni, G.; Rohringer, G.; Toschi, A. Non-perturbative landscape of the Mott-Hubbard transition: Multiple divergence lines around the critical endpoint. *Phys. Rev. B* **2016**, *94*, 235108.

(67) Gunnarsson, O.; Rohringer, G.; Schäfer, T.; Sangiovanni, G.; Toschi, A. Breakdown of Traditional Many-Body Theories for Correlated Electrons. *Phys. Rev. Lett.* **2017**, *119*, 056402.

(68) Maggio, E.; Liu, P.; van Setten, M. J.; Kresse, G. *GW*100: A Plane Wave Perspective for Small Molecules. *J. Chem. Theory Comput.* **2017**, *13*, 635−648.

(69) Golze, D.; Wilhelm, J.; van Setten, M. J.; Rinke, P. Core-Level Binding Energies from *GW*: An Efficient Full-Frequency Approach within a Localized Basis. *J. Chem. Theory Comput.* **2018**, *14*, 4856−4869.

(70) Golze, D.; Keller, L.; Rinke, P. Accurate Absolute and Relative Core-Level Binding Energies from *GW*. *J. Phys. Chem. Lett.* **2020**, *11*, 1840−1847.

(71) Li, J.; Jin, Y.; Rinke, P.; Yang, W.; Golze, D. Benchmark of *GW* Methods for Core-Level Binding Energies. *J. Chem. Theory Comput.* **2022**, *18*, 7570−7585.

(72) Salpeter, E. E.; Bethe, H. A. A Relativistic Equation for Bound-State Problems. *Phys. Rev.* **1951**, *84*, 1232.

(73) Strinati, G. Application of the Green's Functions Method to the Study of the Optical Properties of Semiconductors. *Riv. Nuovo Cimento* **1988**, *11*, 1−86.

(74) Baym, G.; Kadanoff, L. P. Conservation Laws and Correlation Functions. *Phys. Rev.* **1961**, *124*, 287−299.

(75) Baym, G. Self-Consistent Approximations in Many-Body Systems. *Phys. Rev.* **1962**, *127*, 1391−1401.

(76) De Dominicis, C.; Martin, P. C. Stationary Entropy Principle and Renormalization in Normal and Superfluid Systems. I. Algebraic Formulation. *J. Math. Phys.* **1964**, *5*, 14−30.

(77) De Dominicis, C.; Martin, P. C. Stationary Entropy Principle and Renormalization in Normal and Superfluid Systems. II. Diagrammatic Formulation. *J. Math. Phys.* **1964**, *5*, 31−59.

(78) Bickers, N. E.; Scalapino, D. J.; White, S. R. Conserving Approximations for Strongly Correlated Electron Systems: Bethe-Salpeter Equation and Dynamics for the Two-Dimensional Hubbard Model. *Phys. Rev. Lett.* **1989**, *62*, 961−964.

(79) Bickers, N.; Scalapino, D. Conserving approximations for strongly fluctuating electron systems. I. Formalism and calculational approach. *Ann. Phys.* **1989**, *193*, 206−251.

(80) Bickers, N. E.; White, S. R. Conserving approximations for strongly fluctuating electron systems. II. Numerical results and parquet extension. *Phys. Rev. B* **1991**, *43*, 8044−8064.

(81) Hedin, L. On correlation effects in electron spectroscopies and the *GW* approximation. *J. Phys.: Condens. Matter* **1999**, *11*, R489−R528.

(82) Bickers, N. E. Self-Consistent Many-Body Theory for Condensed Matter Systems. In *Theoretical Methods for Strongly Correlated Electrons*; Sénéchal, D., Tremblay, A.-M., Bourbonnais, C., Eds.; Springer: New York, 2004; pp 237−296.

(83) Shirley, E. L. Self-consistent *GW* and higher-order calculations of electron states in metals. *Phys. Rev. B* **1996**, *54*, 7758−7764.

(84) Del Sole, R.; Reining, L.; Godby, R. W. *GW*Γ approximation for electron self-energies in semiconductors and insulators. *Phys. Rev. B* **1994**, *49*, 8024−8028.

(85) Schindlmayr, A.; Godby, R. W. Systematic Vertex Corrections through Iterative Solution of Hedin's Equations Beyond the *GW* Approximation. *Phys. Rev. Lett.* **1998**, *80*, 1702−1705.

(86) Morris, A. J.; Stankovski, M.; Delaney, K. T.; Rinke, P.; García-González, P.; Godby, R. W. Vertex corrections in localized and extended systems. *Phys. Rev. B* **2007**, *76*, 155106.

(87) Shishkin, M.; Marsman, M.; Kresse, G. Accurate Quasiparticle Spectra from Self-Consistent *GW* Calculations with Vertex Corrections. *Phys. Rev. Lett.* **2007**, *99*, 246403.

(88) Romaniello, P.; Guyot, S.; Reining, L. The Self-Energy beyond *GW*: Local and Nonlocal Vertex Corrections. *J. Chem. Phys.* **2009**, *131*, 154111.

(89) Romaniello, P.; Bechstedt, F.; Reining, L. Beyond the G W Approximation: Combining Correlation Channels. *Phys. Rev. B* **2012**, *85*, 155131.

(90) Grüneis, A.; Kresse, G.; Hinuma, Y.; Oba, F. Ionization Potentials of Solids: The Importance of Vertex Corrections. *Phys. Rev. Lett.* **2014**, *112*, 096401.

(91) Maggio, E.; Kresse, G. *GW* Vertex Corrected Calculations for Molecular Systems. *J. Chem. Theory Comput.* **2017**, *13*, 4765−4778.

(92) Mejuto-Zaera, C.; Vlček, V. c. v. Self-consistency in *GW*Γ formalism leading to quasiparticle-quasiparticle couplings. *Phys. Rev. B* **2022**, *106*, 165129.

(93) Lewis, A. M.; Berkelbach, T. C. Vertex Corrections to the Polarizability Do Not Improve the GW Approximation for the

Ionization Potential of Molecules. *J. Chem. Theory Comput.* **2019**, *15*, 2925.

(94) Andersson, K.; Roos, B.; Malmqvist, P. A.; Widmark, P.-O. The Cr_2 Potential Energy Curve Studied with Multiconfigurational Second-Order Perturbation Theory. *Chem. Phys. Lett.* **1994**, *230*, 391−397.

(95) Andersson, K. The Electronic Spectrum of Cr_2. *Chem. Phys. Lett.* **1995**, *237*, 212−221.

(96) Roos, B. O.; Andersson, K. Multiconfigurational Perturbation Theory with Level Shift — the Cr_2 Potential Revisited. *Chem. Phys. Lett.* **1995**, *245*, 215−223.

(97) Forsberg, N.; Malmqvist, P.-Å. Multiconfiguration Perturbation Theory with Imaginary Level Shift. *Chem. Phys. Lett.* **1997**, *274*, 196−204.

(98) Olsen, J.; Jørgensen, P.; Helgaker, T.; Christiansen, O. Divergence in Møller−Plesset Theory: A Simple Explanation Based on a Two-State Model. *J. Chem. Phys.* **2000**, *112*, 9736−9748.

(99) Choe, Y.-K.; Witek, H. A.; Finley, J. P.; Hirao, K. Identifying and Removing Intruder States in Multireference Mo/Ller−Plesset Perturbation Theory. *J. Chem. Phys.* **2001**, *114*, 3913.

(100) Véril, M.; Romaniello, P.; Berger, J. A.; Loos, P. F. Unphysical Discontinuities in *GW* Methods. *J. Chem. Theory Comput.* **2018**, *14*, 5220.

(101) Monino, E.; Loos, P.-F. Unphysical discontinuities, intruder states and regularization in *GW* methods. *J. Chem. Phys.* **2022**, *156*, 231101.

(102) Shishkin, M.; Kresse, G.; Self-Consistent, G. W. Self-Consistent GW Calculations for Semiconductors and Insulators. *Phys. Rev. B* **2007**, *75*, 235102.

(103) Blase, X.; Attaccalite, C.; Olevano, V. First-Principles *GW* Calculations for Fullerenes, Porphyrins, Phtalocyanine, and Other Molecules of Interest for Organic Photovoltaic Applications. *Phys. Rev. B* **2011**, *83*, 115103.

(104) Marom, N.; Caruso, F.; Ren, X.; Hofmann, O. T.; Körzdörfer, T.; Chelikowsky, J. R.; Rubio, A.; Scheffler, M.; Rinke, P. Benchmark of GW Methods for Azabenzenes. *Phys. Rev. B* **2012**, *86*, 245127.

(105) Kaplan, F.; Harding, M. E.; Seiler, C.; Weigend, F.; Evers, F.; van Setten, M. J. Quasi-Particle Self-Consistent *GW* for Molecules. *J. Chem. Theory Comput.* **2016**, *12*, 2528−2541.

(106) Wilhelm, J.; Del Ben, M.; Hutter, J. GW in the Gaussian and Plane Waves Scheme with Application to Linear Acenes. *J. Chem. Theory Comput.* **2016**, *12*, 3623−3635.

(107) Faleev, S. V.; van Schilfgaarde, M.; Kotani, T. All-Electron Self-Consistent G W Approximation: Application to Si, MnO, and NiO. *Phys. Rev. Lett.* **2004**, *93*, 126406.

(108) van Schilfgaarde, M.; Kotani, T.; Faleev, S. Quasiparticle Self-Consistent G W Theory. *Phys. Rev. Lett.* **2006**, *96*, 226402.

(109) Kotani, T.; van Schilfgaarde, M.; Faleev, S. V. Quasiparticle Self-Consistent G W Method: A Basis for the Independent-Particle Approximation. *Phys. Rev. B* **2007**, *76*, 165106.

(110) Ke, S.-H. All-Electron G W Methods Implemented in Molecular Orbital Space: Ionization Energy and Electron Affinity of Conjugated Molecules. *Phys. Rev. B* **2011**, *84*, 205415.

(111) Hybertsen, M. S.; Louie, S. G. First-Principles Theory of Quasiparticles: Calculation of Band Gaps in Semiconductors and Insulators. *Phys. Rev. Lett.* **1985**, *55*, 1418−1421.

(112) von der Linden, W.; Horsch, P. Precise Quasiparticle Energies and Hartree-Fock Bands of Semiconductors and Insulators. *Phys. Rev. B* **1988**, *37*, 8351−8362.

(113) Northrup, J. E.; Hybertsen, M. S.; Louie, S. G. Many-body Calculation of the Surface-State Energies for $Si(111)2 \times 1$. *Phys. Rev. Lett.* **1991**, *66*, 500−503.

(114) Blase, X.; Zhu, X.; Louie, S. G. Self-Energy Effects on the Surface-State Energies of $H-Si(111)1 \times 1$. *Phys. Rev. B* **1994**, *49*, 4973−4980.

(115) Rohlfing, M.; Krüger, P.; Pollmann, J. Efficient Scheme for *GW* Quasiparticle Band-Structure Calculations with Aapplications to Bulk Si and to the $Si(001)-(2 \times 1)$ Surface. *Phys. Rev. B* **1995**, *52*, 1905−1917.

(116) Loos, P. F.; Romaniello, P.; Berger, J. A. Green Functions and Self-Consistency: Insights From the Spherium Model. *J. Chem. Theory Comput.* **2018**, *14*, 3071−3082.

(117) Berger, J. A.; Loos, P.-F.; Romaniello, P. Potential energy surfaces without unphysical discontinuities: the Coulomb-hole plus screened exchange approach. *J. Chem. Theory Comput.* **2021**, *17*, 191.

(118) Di Sabatino, S.; Loos, P.-F.; Romaniello, P. Scrutinizing *GW*-Based Methods Using the Hubbard Dimer. *Front. Chem.* **2021**, *9*, 751054.

(119) Scott, C. J. C.; Backhouse, O. J.; Booth, G. H. A "moment-conserving" reformulation of *GW* theory. *J. Chem. Phys.* **2023**, *158*, 124102.

(120) Lee, J.; Head-Gordon, M. Regularized Orbital-Optimized Second-Order Møller-Plesset Perturbation Theory: A Reliable Fifth-Order-Scaling Electron Correlation Model with Orbital Energy Dependent Regularizers. *J. Chem. Theory Comput.* **2018**, *14*, 5203−5219.

(121) Shee, J.; Loipersberger, M.; Rettig, A.; Lee, J.; Head-Gordon, M. Regularized Second-Order Møller−Plesset Theory: A More Accurate Alternative to Conventional MP2 for Noncovalent Interactions and Transition Metal Thermochemistry for the Same Computational Cost. *J. Phys. Chem. Lett.* **2021**, *12*, 12084−12097.

(122) Evangelista, F. A. A driven similarity renormalization group approach to quantum many-body problems. *J. Chem. Phys.* **2014**, *141*, 054109.

(123) Li, C.; Evangelista, F. A. Multireference Theories of Electron Correlation Based on the Driven Similarity Renormalization Group. *Annu. Rev. Phys. Chem.* **2019**, *70*, 245−273.

(124) Battaglia, S.; Fransén, L.; Fdez. Galván, I.; Lindh, R. Regularized CASPT2: An Intruder-State-Free Approach. *J. Chem. Theory Comput.* **2022**, *18*, 4814−4825.

(125) Coveney, C. J. N.; Tew, D. P. A Regularized Second-Order Correlation Method from Green's Function Theory. 2023, arXiv:2302.13296. *arXiv Preprint.* https://arxiv.org/abs/2302.13296 (accessed 2023-06-05).

(126) Wegner, F. Flow-equations for Hamiltonians. *Ann. Phys. Leipzig* **1994**, *506*, 77.

(127) Głazek, S. D.; Wilson, K. G. Renormalization of Hamiltonians. *Phys. Rev. D* **1993**, *48*, 5863−5872.

(128) Glazek, S. D.; Wilson, K. G. Perturbative renormalization group for Hamiltonians. *Phys. Rev. D* **1994**, *49*, 4214−4218.

(129) White, S. R. Numerical canonical transformation approach to quantum many-body problems. *J. Chem. Phys.* **2002**, *117*, 7472−7482.

(130) Li, C.; Evangelista, F. A. Multireference Driven Similarity Renormalization Group: A Second-Order Perturbative Analysis. *J. Chem. Theory Comput.* **2015**, *11*, 2097−2108.

(131) Li, C.; Evangelista, F. A. Towards Numerically Robust Multireference Theories: The Driven Similarity Renormalization Group Truncated to One- and Two-Body Operators. *J. Chem. Phys.* **2016**, *144*, 164114.

(132) Li, C.; Evangelista, F. A. Driven Similarity Renormalization Group: Third-order Multireference Perturbation Theory. *J. Chem. Phys.* **2017**, *146*, 124132.

(133) Li, C.; Evangelista, F. A. Driven Similarity Renormalization Group for Excited States: A State-Averaged Perturbation Theory. *J. Chem. Phys.* **2018**, *148*, 124106.

(134) Zhang, T.; Li, C.; Evangelista, F. A. Improving the Efficiency of the Multireference Driven Similarity Renormalization Group via Sequential Transformation, Density Fitting, and the Noninteracting Virtual Orbital Approximation. *J. Chem. Theory Comput.* **2019**, *15*, 4399−4414.

(135) Li, C.; Evangelista, F. A. Spin-free formulation of the multireference driven similarity renormalization group: A benchmark study of first-row diatomic molecules and spin-crossover energetics. *J. Chem. Phys.* **2021**, *155*, 114111.

(136) Wang, S.; Li, C.; Evangelista, F. A. Analytic Energy Gradients for the Driven Similarity Renormalization Group Multireference Second-Order Perturbation Theory. *J. Chem. Theory Comput.* **2021**, *17*, 7666−7681.

(137) Wang, M.; Fang, W.-H.; Li, C. Assessment of State-Averaged Driven Similarity Renormalization Group on Vertical Excitation Energies: Optimal Flow Parameters and Applications to Nucleobases. *J. Chem. Theory Comput.* **2023**, *19*, 122−136.

(138) Bogner, S. K.; Furnstahl, R. J.; Perry, R. J. Similarity Renormalization Group for Nucleon-Nucleon Interactions. *Phys. Rev. C* **2007**, *75*, 061001.

(139) Tsukiyama, K.; Bogner, S. K.; Schwenk, A. In-Medium Similarity Renormalization Group For Nuclei. *Phys. Rev. Lett.* **2011**, *106*, 222502.

(140) Tsukiyama, K.; Bogner, S. K.; Schwenk, A. In-Medium Similarity Renormalization Group for Open-Shell Nuclei. *Phys. Rev. C* **2012**, *85*, 061304.

(141) Hergert, H.; Bogner, S. K.; Binder, S.; Calci, A.; Langhammer, J.; Roth, R.; Schwenk, A. In-Medium Similarity Renormalization Group with Chiral Two- plus Three-Nucleon Interactions. *Phys. Rev. C* **2013**, *87*, 034307.

(142) Hergert, H. In-Medium Similarity Renormalization Group for Closed and Open-Shell Nuclei. *Phys. Scr.* **2017**, *92*, 023002.

(143) Frosini, M.; Duguet, T.; Ebran, J.-P.; Somà, V. Multi-Reference Many-Body Perturbation Theory for Nuclei. *Eur. Phys. J. A* **2022**, *58*, 62.

(144) Frosini, M.; Duguet, T.; Ebran, J.-P.; Bally, B.; Mongelli, T.; Rodríguez, T. R.; Roth, R.; Somà, V. Multi-Reference Many-Body Perturbation Theory for Nuclei. *Eur. Phys. J. A* **2022**, *58*, 63.

(145) Frosini, M.; Duguet, T.; Ebran, J.-P.; Bally, B.; Hergert, H.; Rodríguez, T. R.; Roth, R.; Yao, J. M.; Somà, V. Multi-Reference Many-Body Perturbation Theory for Nuclei. *Eur. Phys. J. A* **2022**, *58*, 64.

(146) Casida, M. E.; Chong, D. P. Physical Interpretation and Assessment of the Coulomb-Hole and Screened-Exchange Approximation for Molecules. *Phys. Rev. A* **1989**, *40*, 4837−4848.

(147) Casida, M. E.; Chong, D. P. Simplified Green-Function Approximations: Further Assessment of a Polarization Model for Second-Order Calculation of Outer-Valence Ionization Potentials in Molecules. *Phys. Rev. A* **1991**, *44*, 5773−5783.

(148) Szabo, A.; Ostlund, N. S. *Modern quantum chemistry*; McGraw-Hill: New York, 1989.

(149) Stefanucci, G.; van Leeuwen, R. *Nonequilibrium Many-Body Theory of Quantum Systems: A Modern Introduction*; Cambridge University Press: Cambridge, 2013.

(150) Ortiz, J. V. Electron Propagator Theory: An Approach to Prediction and Interpretation in Quantum Chemistry: Electron Propagator Theory. *Wiley Interdiscip. Rev. Comput. Mol. Sci.* **2013**, *3*, 123−142.

(151) Phillips, J. J.; Zgid, D. Communication: The Description of Strong Correlation within Self-Consistent Green's Function Second-Order Perturbation Theory. *J. Chem. Phys.* **2014**, *140*, 241101.

(152) Phillips, J. J.; Kananenka, A. A.; Zgid, D. Fractional Charge and Spin Errors in Self-Consistent Green's Function Theory. *J. Chem. Phys.* **2015**, *142*, 194108.

(153) Rusakov, A. A.; Phillips, J. J.; Zgid, D. Local Hamiltonians for Quantitative Green's Function Embedding Methods. *J. Chem. Phys.* **2014**, *141*, 194105.

(154) Rusakov, A. A.; Zgid, D. Self-Consistent Second-Order Green's Function Perturbation Theory for Periodic Systems. *J. Chem. Phys.* **2016**, *144*, 054106.

(155) Hirata, S.; Hermes, M. R.; Simons, J.; Ortiz, J. V. General-Order Many-Body Green's Function Method. *J. Chem. Theory Comput.* **2015**, *11*, 1595−1606.

(156) Hirata, S.; Doran, A. E.; Knowles, P. J.; Ortiz, J. V. One-Particle Many-Body Green's Function Theory: Algebraic Recursive Definitions, Linked-Diagram Theorem, Irreducible-Diagram Theorem, and General-Order Algorithms. *J. Chem. Phys.* **2017**, *147*, 044108.

(157) Backhouse, O. J.; Santana-Bonilla, A.; Booth, G. H. Scalable and Predictive Spectra of Correlated Molecules with Moment Truncated Iterated Perturbation Theory. *J. Phys. Chem. Lett.* **2021**, *12*, 7650−7658.

(158) Backhouse, O. J.; Booth, G. H. Efficient Excitations and Spectra within a Perturbative Renormalization Approach. *J. Chem. Theory Comput.* **2020**, *16*, 6294−6304.

(159) Backhouse, O. J.; Nusspickel, M.; Booth, G. H. Wave Function Perspective and Efficient Truncation of Renormalized Second-Order Perturbation Theory. *J. Chem. Theory Comput.* **2020**, *16*, 1090−1104.

(160) Pokhilko, P.; Zgid, D. Interpretation of multiple solutions in fully iterative GF2 and *GW* schemes using local analysis of two-particle density matrices. *J. Chem. Phys.* **2021**, *155*, 024101.

(161) Pokhilko, P.; Iskakov, S.; Yeh, C.-N.; Zgid, D. Evaluation of two-particle properties within finite-temperature self-consistent one-particle Green's function methods: Theory and application to *GW* and GF2. *J. Chem. Phys.* **2021**, *155*, 024119.

(162) Pokhilko, P.; Yeh, C.-N.; Zgid, D. Iterative subspace algorithms for finite-temperature solution of Dyson equation. *J. Chem. Phys.* **2022**, *156*, 094101.

(163) Liebsch, A. Ni *d*-band self-energy beyond the low-density limit. *Phys. Rev. B* **1981**, *23*, 5203−5212.

(164) Katsnelson, M. I.; Lichtenstein, A. I. LDA++ approach to the electronic structure of magnets: correlation effects in iron. *J. Phys.: Condens. Matter* **1999**, *11*, 1037−1048.

(165) Katsnelson, M.; Lichtenstein, A. Electronic structure and magnetic properties of correlated metals. *Eur. Phys. J. B* **2002**, *30*, 9−15.

(166) Zhukov, V. P.; Chulkov, E. V.; Echenique, P. M. GW + T Theory of Excited Electron Lifetimes in Metals. *Phys. Rev. B* **2005**, *72*, 155109.

(167) Puig von Friesen, M.; Verdozzi, C.; Almbladh, C.-O. Kadanoff-Baym dynamics of Hubbard clusters: Performance of many-body schemes, correlation-induced damping and multiple steady and quasi-steady states. *Phys. Rev. B* **2010**, *82*, 155108.

(168) Gukelberger, J.; Huang, L.; Werner, P. On the dangers of partial diagrammatic summations: Benchmarks for the two-dimensional Hubbard model in the weak-coupling regime. *Phys. Rev. B* **2015**, *91*, 235114.

(169) Müller, M. C. T. D.; Blügel, S.; Friedrich, C. Electron-magnon scattering in elementary ferromagnets from first principles: Lifetime broadening and band anomalies. *Phys. Rev. B* **2019**, *100*, 045130.

(170) Friedrich, C. Tetrahedron integration method for strongly varying functions: Application to the *GT* self-energy. *Phys. Rev. B* **2019**, *100*, 075142.

(171) Biswas, T.; Singh, A. Excitonic effects in absorption spectra of carbon dioxide reduction photocatalysts. *npj Comput. Mater.* **2021**, *7*, 189.

(172) Zhang, D.; Su, N. Q.; Yang, W. Accurate Quasiparticle Spectra from the T-Matrix Self-Energy and the Particle−Particle Random Phase Approximation. *J. Phys. Chem. Lett.* **2017**, *8*, 3223−3227.

(173) Li, J.; Chen, Z.; Yang, W. Renormalized Singles Green's Function in the T-Matrix Approximation for Accurate Quasiparticle Energy Calculation. *J. Phys. Chem. Lett.* **2021**, *12*, 6203−6210.

(174) Loos, P.-F.; Romaniello, P. Static and dynamic Bethe-Salpeter equations in the T-matrix approximation. *J. Chem. Phys.* **2022**, *156*, 164101.

(175) Tiago, M. L.; Chelikowsky, J. R. Optical Excitations in Organic Molecules, Clusters, and Defects Studied by First-Principles Green's Function Methods. *Phys. Rev. B* **2006**, *73*, 205334.

(176) Bruneval, F. Ionization Energy of Atoms Obtained from *GW* Self-Energy or from Random Phase Approximation Total Energies. *J. Chem. Phys.* **2012**, *136*, 194107.

(177) van Setten, M. J.; Weigend, F.; Evers, F. The *GW*-Method for Quantum Chemistry Applications: Theory and Implementation. *J. Chem. Theory Comput.* **2013**, *9*, 232−246.

(178) Bruneval, F.; Rangel, T.; Hamed, S. M.; Shao, M.; Yang, C.; Neaton, J. B. Molgw 1: Many-Body Perturbation Theory Software for Atoms, Molecules, and Clusters. *Comput. Phys. Commun.* **2016**, *208*, 149−161.

(179) Körzdörfer, T.; Marom, N. Strategy for Finding a Reliable Starting Point for ${G_{0}W_{0}}$ Demonstrated for Molecules. *Phys. Rev. B* **2012**, *86*, 041110.

(180) Bruneval, F.; Marques, M. A. L. Benchmarking the Starting Points of the GW Approximation for Molecules. *J. Chem. Theory Comput.* **2013**, *9*, 324−329.

(181) Gallandi, L.; Körzdörfer, T. Long-Range Corrected DFT Meets GW: Vibrationally Resolved Photoelectron Spectra from First Principles. *J. Chem. Theory Comput.* **2015**, *11*, 5391–5400.

(182) Gallandi, L.; Marom, N.; Rinke, P.; Körzdörfer, T. Accurate Ionization Potentials and Electron Affinities of Acceptor Molecules II: Non-Empirically Tuned Long-Range Corrected Hybrid Functionals. *J. Chem. Theory Comput.* **2016**, *12*, 605–614.

(183) Lei, J.; Zhu, T. Gaussian-Based Quasiparticle Self-Consistent GW for Periodic Systems. *J. Chem. Phys.* **2022**, *157*, 214114.

(184) Ismail-Beigi, S. Justifying Quasiparticle Self-Consistent Schemes via Gradient Optimization in Baym–Kadanoff Theory. *J. Phys. Cond. Mater.* **2017**, *29*, 385501.

(185) Surján, P. R.; Szabados, Á. Damping of Perturbation Corrections in Quasidegenerate Situations. *J. Chem. Phys.* **1996**, *104*, 3320–3324.

(186) Stück, D.; Head-Gordon, M. Regularized orbital-optimized second-order perturbation theory. *J. Chem. Phys.* **2013**, *139*, 244109.

(187) Razban, R. M.; Stück, D.; Head-Gordon, M. Addressing first derivative discontinuities in orbital-optimized opposite-spin scaled second-order perturbation theory with regularisation. *Mol. Phys.* **2017**, *115*, 2102–2109.

(188) Kehrein, S. *The Flow Equation Approach to Many-Particle Systems*; Springer Tracts in Modern Physics; Springer Berlin/Heidelberg: 2006; Vol. *217*.

(189) Evangelista, F. A. Adaptive multiconfigurational wave functions. *J. Chem. Phys.* **2014**, *140*, 124114.

(190) Bintrim, S. J.; Berkelbach, T. C. Full-frequency GW without frequency. *J. Chem. Phys.* **2021**, *154*, 041101.

(191) Tölle, J.; Chan, G. K.-L. Exact relationships between the GW approximation and equation-of-motion coupled-cluster theories through the quasi-boson formalism. *J. Chem. Phys.* **2023**, *158*, 124123.

(192) Löwdin, P. Studies in perturbation theory: Part I. An elementary iteration-variation procedure for solving the Schrödinger equation by partitioning technique. *J. Mol. Spectrosc.* **1963**, *10*, 12–33.

(193) Loos, P.-F.; Scemama, A.; Jacquemin, D. The Quest for Highly Accurate Excitation Energies: A Computational Perspective. *J. Phys. Chem. Lett.* **2020**, *11*, 2374–2383.

(194) Véril, M.; Scemama, A.; Caffarel, M.; Lipparini, F.; Boggio-Pasqua, M.; Jacquemin, D.; Loos, P.-F. QUESTDB: A database of highly accurate excitation energies for the electronic structure community. *WIREs Comput. Mol. Sci.* **2021**, *11*, e1517.

(195) Christiansen, O.; Koch, H.; Jørgensen, P. Response Functions in the CC3 Iterative Triple Excitation Model. *J. Chem. Phys.* **1995**, *103*, 7429–7441.

(196) Koch, H.; Christiansen, O.; Jorgensen, P.; Sanchez de Merás, A. M.; Helgaker, T. The CC3Model: An Iterative Coupled Cluster Approach Including Connected Triples. *J. Chem. Phys.* **1997**, *106*, 1808–1818.

(197) Matthews, D. A.; Cheng, L.; Harding, M. E.; Lipparini, F.; Stopkowicz, S.; Jagau, T.-C.; Szalay, P. G.; Gauss, J.; Stanton, J. F. Coupled-Cluster Techniques for Computational Chemistry: The CFOUR Program Package. *J. Chem. Phys.* **2020**, *152*, 214108.

(198) Loos, P. F. QuAcK: a software for emerging quantum electronic structure methods. 2019. https://github.com/pfloos/QuAcK (accessed 2023-06-05).

(199) Pulay, P. Convergence Acceleration of Iterative Sequences. the Case of Scf Iteration. *Chem. Phys. Lett.* **1980**, *73*, 393–398.

(200) Pulay, P. ImprovedSCF Convergence Acceleration. *J. Comput. Chem.* **1982**, *3*, 556–560.

(201) Frisch, M. J.; Trucks, G. W.; Schlegel, H. B.; Scuseria, G. E.; Robb, M. A.; Cheeseman, J. R.; Scalmani, G.; Barone, V.; Petersson, G. A.; Nakatsuji, H.; Li, X.; Caricato, M.; Marenich, A. V.; Bloino, J.; Janesko, B. G.; Gomperts, R.; Mennucci, B.; Hratchian, H. P.; Ortiz, J. V.; Izmaylov, A. F.; Sonnenberg, J. L.; Williams-Young, D.; Ding, F.; Lipparini, F.; Egidi, F.; Goings, J.; Peng, B.; Petrone, A.; Henderson, T.; Ranasinghe, D.; Zakrzewski, V. G.; Gao, J.; Rega, N.; Zheng, G.; Liang, W.; Hada, M.; Ehara, M.; Toyota, K.; Fukuda, R.; Hasegawa, J.; Ishida, M.; Nakajima, T.; Honda, Y.; Kitao, O.; Nakai, H.; Vreven, T.; Throssell, K.; Montgomery, J. A., Jr.; Peralta, J. E.; Ogliaro, F.; Bearpark, M. J.; Heyd, J. J.; Brothers, E. N.; Kudin, K. N.; Staroverov, V. N.; Keith, T. A.; Kobayashi, R.; Normand, J.; Raghavachari, K.; Rendell, A. P.; Burant, J. C.; Iyengar, S. S.; Tomasi, J.; Cossi, M.; Millam, J. M.; Klene, M.; Adamo, C.; Cammi, R.; Ochterski, J. W.; Martin, R. L.; Morokuma, K.; Farkas, O.; Foresman, J. B.; Fox, D. J. *Gaussian 16*, Revision C.01; Gaussian Inc.: Wallingford, CT, 2016.

(202) Schirmer, J. *Many-Body Methods for Atoms, Molecules and Clusters*; Springer: 2018.

(203) Richard, R. M.; Marshall, M. S.; Dolgounitcheva, O.; Ortiz, J. V.; Brédas, J.-L.; Marom, N.; Sherrill, C. D. Accurate Ionization Potentials and Electron Affinities of Acceptor Molecules I. Reference Data at the CCSD(T) Complete Basis Set Limit. *J. Chem. Theory Comput.* **2016**, *12*, 595–604.

(204) Knight, J. W.; Wang, X.; Gallandi, L.; Dolgounitcheva, O.; Ren, X.; Ortiz, J. V.; Rinke, P.; Körzdörfer, T.; Marom, N. Accurate Ionization Potentials and Electron Affinities of Acceptor Molecules III: A Benchmark of GW Methods. *J. Chem. Theory Comput.* **2016**, *12*, 615–626.

(205) Dolgounitcheva, O.; Díaz-Tinoco, M.; Zakrzewski, V. G.; Richard, R. M.; Marom, N.; Sherrill, C. D.; Ortiz, J. V. Accurate Ionization Potentials and Electron Affinities of Acceptor Molecules IV: Electron-Propagator Methods. *J. Chem. Theory Comput.* **2016**, *12*, 627–637.

⬡ Recommended by ACS